Secondary organic aerosol from biomass burning phenolic compounds and nitrate radicals can be highly viscous over a wide relative humidity range

Sepehr Nikkho[1], Bin Bai[2], Fabian Mahrt[1, 3, †], Julia Zaks[1], Long Peng[1, ‡], Kristian J. Kiland[1, §], Pengfei Liu[2], and Allan K. Bertram[1, *]

[1] Department of Chemistry, The University of British Columbia, Vancouver, British Columbia, V6T 1Z1, Canada

[2] School of Earth and Atmospheric Sciences, Georgia Institute of Technology, Atlanta, GA, 30332, USA

[3] Laboratory of Atmospheric Chemistry, Paul Scherrer Institute, Forschungsstrasse 111, 5232 Villigen, Switzerland

[†] Now at: Department of Chemistry, Aarhus University, 8000 Aarhus, Denmark

[‡] Now at: College of Ecology and Environment, Xinjiang University, Urumqi 830017, China

[§] Now at: Department of Integrative Oncology, British Columbia Cancer Research Institute, Vancouver British Columbia, V5Z 1L3, Canada

[*] Corresponding author

Abstract

Biomass burning events, including wildfires, can emit large amounts of phenolic compounds such as guaiacol. These phenolic compounds can undergo oxidation by nitrate radicals (NO_3) to form secondary organic aerosol (SOA). Viscosity and hygroscopicity are key properties that affect SOA's role in atmospheric chemistry, air quality, and climate. However, these properties have not been quantified for SOA formed from the reaction of phenolic compounds with NO_3. We used the poke-flow technique and a quartz crystal microbalance (QCM) to measure the viscosity and hygroscopicity of SOA particles generated from the reaction of NO_3 with guaiacol, termed guaiacol-NO_3 SOA. The viscosity of this SOA is extremely high ($\gtrsim 5\times10^7$ Pa s) at RH $\lesssim$ 70% and drastically higher than previously reported for other SOA types investigated with the poke-flow technique at RH $\gtrsim$ 40%. The high viscosity for guaiacol-NO_3 SOA can be attributed, at least in part, to the low hygroscopicity measured by the QCM. From the viscosity results, we calculated the mixing times of organic molecules within guaiacol-NO_3 SOA. The results suggest that mixing times within guaiacol-NO_3 SOA particles with atmospherically relevant sizes exceed 1 hour for most tropospheric conditions, with possible implications for predicting the size, mass, and long-range transport of pollutants in phenolic SOA.

1. Introduction

Biomass burning events, including wildfires, can emit large amounts of phenolic compounds, such as guaiacol, catechol, and syringol into the atmosphere.[1–5] Once in the atmosphere, phenolic compounds can be oxidized by hydroxyl radicals (OH), ozone (O_3), and nitrate radicals (NO_3) to form lower volatility products, which can partition to the particle phase, forming secondary organic aerosol (SOA).[2,6–17] OH and O_3 are the main oxidants during the day, while NO_3 and O_3 are the main oxidants during the night or during the day in light-limited environments, such as within dense biomass burning plumes.[16,18] A recent study suggests that oxidation of biomass burning plumes by NO_3 during the night can lead to rapid production of SOA in the atmosphere.[19]

SOA, including phenolic SOA can impact climate indirectly by acting as cloud condensation nuclei and possibly ice nucleating particles, thereby changing the reflectivity and lifetime of clouds.[20–23] In addition, SOA can contribute to poor air quality and negatively impact human health.[24–26]

Viscosity is a physiochemical property of SOA that is important for predicting its impact on climate and air quality.[27] Viscosity is inversely related to molecular diffusion rates within SOA particles, based on the Stokes-Einstein equation.[28] As a result, viscosity can impact gas-particle partitioning and the mass and size distributions of SOA in the atmosphere.[29–40] In addition, viscosity can affect the rates and mechanisms of multiphase reactions within SOA particles[36,41–53] and the long-range transport of particle-borne pollutants like polycyclic aromatic hydrocarbons.[41,54–57] Some studies have also suggested that highly viscous SOA can act as heterogeneous nuclei for ice formation in the atmosphere,[23,58–63], although the importance of the glassy phase state for ice nucleation is still a matter of debate.[64]

Many studies have quantified the viscosity of SOA generated with OH or O_3. In addition, two studies investigated the viscosity of phenolic SOA generated using OH or O_3 as the oxidants. [65,66] In contrast, much less is known on the viscosity of SOA, either phenolic or other types, formed with NO_3.

Kasparoglu et al. suggested that SOA generated from the oxidation of α-pinene by NO_3 was viscous or hydrophobic or both, based on ice nucleation measurements.[64] In addition, experiments

by Perraud et al. suggested that SOA generated from the oxidation of α-pinene by a combination of O_3 and NO_3 is highly viscous, based on the non-equilibrium partitioning of organic nitrates.[67]

Field measurements have also suggested that atmospheric aerosol particles can be more viscous at night compared to the day.[68,69] Slade et al. found this to be true for aerosol particles in a forest environment.[68] Differences were attributed to terpene-derived, higher molecular weight SOA at night and isoprene-derived, lower molecular weight SOA during the day. Bateman et al. studied anthropogenic emissions in the Amazon and observed an increase in particle rebound fraction in an impactor at night, which is associated with more viscous particles.[69]

Hygroscopicity is another key physiochemical property of SOA that is important for predicting its climate impact.[70,71] Hygroscopicity determines the water content of the particles, and hence their light scattering properties and ability to act as nuclei for cloud droplets.[70–72] Hygroscopicity also impacts the viscosity of SOA.[73–78] Consider for example an SOA type that has a high hygroscopicity and a high viscosity under dry conditions, such as SOA generated by OH oxidation of toluene.[52,79,80] For this system, as the relative humidity (RH) increases, the SOA particles will take up water and the overall viscosity will decrease[52,79,80] since water has a lower viscosity than dry SOA.[78]

The hygroscopicity of SOA generated from O_3 or OH has been extensively studied.[81–84] In addition, there have been some studies on the hygroscopicity of phenolic SOA and proxies for phenolic SOA.[85–88] In comparison, there have been fewer studies on the hygroscopicity of SOA generated by NO_3,[89–91] and we are not aware of any research that has quantified the hygroscopicity of phenolic SOA generated with NO_3 as the oxidant.

Here, we measured the RH-dependent viscosity of SOA particles at 294 K generated by reacting NO_3 with guaiacol (2-methoxyphenol), referred to as guaiacol-NO_3 SOA. Guaiacol, a phenolic compound, is emitted from biomass burning events and can contribute significantly to SOA formation in the atmosphere.[2,11,14,16,17,92–95] We use guaiacol as a model system for phenolic compounds from biomass burning events. We found that the viscosity of this SOA is extremely high ($\gtrsim 5\times10^7$ Pa s) at RH $\lesssim$ 70%. In addition to measuring the RH-dependent viscosity of guaiacol-NO_3 SOA, we also developed a parameterization for predicting the viscosity of this SOA

as a function of RH and temperature, and used this parameterization to predict the viscosity and mixing times within phenolic SOA in the atmosphere.

We also measured the hygroscopicity of the guaiacol-NO_3 SOA to better understand the high viscosities of this SOA type. For comparison purposes, we also measured the hygroscopicity of guaiacol-OH SOA. The results suggest that phenolic SOA generated by NO_3 during the night can have a much higher viscosity than phenolic SOA generated by OH during the day, and the differences can be explained, at least partially, by the low hygroscopicity of the guaiacol-NO_3 SOA.

2. Materials and Methods

2.1. Production of Guaiacol-NO_3 SOA

Guaiacol-NO_3 SOA was generated in an environmental chamber (Fig. 1) consisting of a 1.8 m^3 Teflon bag (Ingeniven) suspended within an aluminum enclosure and surrounded by 24 UV lights (Sylvania Black lights, 40 W λ ~360 nm).[96] The chamber was cleaned with deionized water and then flushed with zero-air (Aadco 737) for 48 h while the UV lights were on. SOA generation was carried out in the continuous flow mode at 294 K, in the dark, and under dry conditions ($\lesssim$ 1% RH). The total flow rate through the environmental chamber was ~16 L min^{-1}, corresponding to an average residence time of ~112 min, calculated assuming plug flow. SOA was produced without seed particles to prevent their influence on the viscosity and hygroscopicity measurements.

Organic vapors were added to the environmental chamber by continuously injecting a solution of 2 wt. % guaiacol (Sigma Aldrich, purity ≥ 99.9%) in ultrapure water (Merck Millipore, Milli-Q,) into a round bottom glass flask. The flask was heated to ~323 K to enhance vaporization. The resulting vapors were carried into the environmental chamber by continuously flushing the flask with zero-air. Prior to reaction, the concentration of guaiacol in the environmental chamber was ~50 ppb.

NO_3 was generated within the environmental chamber by the thermal decomposition of dinitrogen pentoxide (N_2O_5). N_2O_5 was generated upstream of the environmental chamber by reacting O_3 and NO_2 in a flow reactor (Fig. 1), following established methods.[97,98] The flow reactor consisted

of four large glass vessels coupled in series with an overall volume of 60 L. The average residence time within the flow reactor was ~39 minutes, assuming plug flow. The following reactions occurred within the flow reactor:

$$NO_2+O_3 \rightarrow NO_3+O_2 \quad R_1$$

$$NO_2+NO_3 \rightarrow N_2O_5 \quad R_2$$

$$N_2O_5 \rightarrow NO_2+NO_3 \quad R_3$$

The O_3 for reaction R_1 was generated upstream of the flow reactor by continuously passing zero-air through an ozone generator (Jelight, model: 600). NO_2 was continuously added to the flow reactor from a cylinder (806 ppm NO_2 in nitrogen gas). The concentration of NO_2 and O_3 in the flow reactor were measured with a NO_x analyzer (Thermo Scientific, 42i NO_x) and an O_3 analyzer (Thermo Scientific, 49i), respectively. The ratio of NO_2: O_3 before reaction in the flow reactor was ~2:1. The gas-phase rate constants for these reactions are shown in Table S1.

We employed a MATLAB-based kinetic model (Supporting Information, Section S1) to assess NO_3 and N_2O_5 concentrations in the flow reactor and the environmental chamber (Figs. S1 and S2). Based on these simulations, prior to reaction with guaiacol, NO_3 and N_2O_5 levels in the chamber were around 460 ppt and 220 ppb, respectively. Additionally, the thermal decomposition of N_2O_5 continuously supplied NO_3 within the environmental chamber as guaiacol reacted with NO_3. Based on the kinetic model, greater than 99.9% of guaiacol reacted with NO_3, while the rest reacted with O_3.

The generated SOA mass concentration at the chamber exit was measured using an optical particle counter (GRIMM, 11-S OPC), averaging 40-100 μg m^{-3} for the experiments discussed herein. For viscosity measurements, SOA was collected onto glass slides with hydrophobic and oleophobic coatings (CYTONIX, FluoroPel 800). SOA collection was carried out using a multi-orifice single-stage impactor (Moudi, Model 100-180nm-10LPM). Since long collection times were used, SOA that impacted on the hydrophobic and oleophobic slides coagulated to form super-micrometer particles (50-100 μm diameter). For hygroscopicity measurements, SOA was collected on Teflon filters (Sartorius PTFE Membrane Filters, pore size of 5 μm) at a flow rate of ~12 L min^{-1} for 3-6 h each. Filters were stored at -18 °C in air-tight containers prior to analysis.

We used a high-resolution time-of-flight aerosol mass spectrometer (HR-ToF-AMS) from Aerodyne Research[99] to probe the composition of the guaiacol-NO_3 SOA. The amount of nitrogen-containing compounds in the mass spectrum was 15% (Section S2 and Fig. S3), consistent with expectations based on previous HR-AMS measurements of SOA generated by reactions of NO_3 with volatile organic compounds.[66,100] As expected for this reaction, all of the nitrogen-containing compounds identified in the mass spectrometer originated from organic nitrogen compounds. For details, see Section S2.

2.2. Production of Guaiacol-OH SOA

Guaiacol-OH SOA was generated using the same environmental chamber described above and similar experimental conditions described in Kiland et al.[65] Briefly, the chamber was operated in continuous flow mode, with a total flow rate of ~19.2 L min^{-1}. A solution of guaiacol (2 wt. %) in MilliQ water was injected into a heated round bottom glass flask, and the vaporized solution was flushed into the environmental chamber. OH was generated by the photolysis of H_2O_2 using 24 UV lights (Sylvania Black lights, 40 W λ ~360 nm). $H_2O_2$was added to the environmental chamber by continuously injecting a solution of H_2O_2 (Sigma-Aldrich, 30 wt. % in water) into a heated round bottom glass flask, and the resulting vapors were flushed into the chamber with zero air. The mass concentration of SOA at the exit of the chamber was 50-70 μg m^{-3}. The SOA was collected in a similar fashion as described in Sect. 2.1.

2.3. Hygroscopicity Measurements

Hygroscopicity of the SOA particles collected on the Teflon filter was measured using a Quartz Crystal Microbalance (QCM). After collection, a piece of SOA-laden filter was pressed on the surface of a clean QCM sensor (Novaetech, AT5-14-12-AU). The filter was then peeled off, leaving a thin film of SOA remaining on the sensor surface. After preparation, the QCM crystals were mounted in a temperature-controlled flow module (Q-sense, QFM401) and purged with zero air at a total flow rate of 30 cm^3 min^{-1}. The RH in the flow cell was switched between dry (< 1% RH) and humidified (10–95% RH) conditions by changing the mixing ratio of dry and humidified pure air flows using two mass flow controllers. An RH sensor (Rotronic, HC2A-S) continuously monitored the RH in the cell. The QCM (Q-sense Explorer) continuously monitored the mass of SOA film, as described elsewhere.[80]

The SOA mass at the dry condition (< 1% RH) was measured before and after the measurement at an elevated RH, and possible evaporation of dry organic material was accounted for (e.g. SI, Fig. S4). The mass sensitivity of the QCM was < 1 ng cm^{-2}, corresponding to one-tenth of a single molecule-layer of water. This sensitivity was sufficient for accurately detecting water uptake at RH values > 10%. The adsorption of water vapor on a blank sensor surface was determined and subtracted from the hygroscopic growth calculation (SI, Fig. S5). From the QCM measurements, we determined the mass-based hygroscopic growth factor, which is the ratio of the particle mass at a specific RH to the particle mass under dry condition. In addition, we determined the mass-based hygroscopicity parameter (κ_m) using the following equation:[72]

$$\kappa_m=(\frac{100}{RH}-1)\frac{m_w}{m_d} \quad \text{Eq. 1}$$

where m_w and m_d is the mass of water and dry SOA, respectively, and RH is the relative humidity.

The QCM method for hygroscopicity measurements was validated by experiments using amorphous sucrose thin films in our previous study, which shows good agreement with results derived from other methods.[101]

2.4. Viscosity Measurement

The viscosity of the super-micrometer SOA particles was determined using the poke-flow technique described in detail previously.[102–104] A hydrophobic slide containing SOA particles was placed inside a RH-controlled flow cell that was coupled to an inverted optical microscope (AmScope, ME1400TC-INF, Fig. S6a). To control the RH within the flow cell, dry and/or humidified zero-air was continuously flowed through the cell. The dew point of the air was measured by a chilled mirror hygrometer (General Eastern, 1311DR-SR-115V) mounted downstream of the flow cell. The temperature of the cell was monitored by a thermocouple (OMEGA, HH-200a) probe connected to the flow cell, and was approximately 294 K for all measurements reported here. The RH within the cell was calculated from the dew point of the air and temperature of the cell.

Prior to poking the particles, the particles were conditioned to the RH within the flow cell. After conditioning, the particles were poked with an ultra-fine tungsten needle (Roboz Surgical Instruments Co., Fig. S6). The needle was coated with an oleophobic solution (CYTONIX, OilSlip

110) and was mounted on a micromanipulator (Narishige; model MO-202), which enables high-precision three-dimensional movement of the needle. Upon poking the particle, a non-equilibrium geometry was generated (Fig. S6b). After retrieving the needle from the particle, the SOA material flowed (unless the viscosity was very high) and returned to initial equilibrium geometry, i.e. spherical cap geometry, to minimize the surface energy of the system.[103] At high RH values ($\gtrsim$ 70%), the particle formed a roughly half-torus geometry after poking (e.g. Fig. 2, 2nd and 3rd row). From the images recorded when the SOA material flowed, we determined the time required for the inner diameter of the half-torus shape to reduce by ~50% of its initial value, which we term the experimental flow time $\tau_{exp,flow}$. For RH values $\lesssim$ 60%, the particles cracked and did not flow during the observation time (e.g. Fig. 2, 1st row). In these cases the observation time was used as a lower limit to $\tau_{exp,flow}$.

To convert $\tau_{exp,flow}$ to viscosity we used fluid dynamics simulations of the poked particles, carried out using a microfluidics module within COMSOL Multiphysics (COMOSL Inc., v5.4). The simulations took into account the Navier–Stokes momentum equation and the continuity equation. For particles that formed an approximately half-torus geometry after poking, a half-torus geometry was used in the simulations. Upper and lower limits for the particle's surface tension, contact angle, and Navier slip length (Table S2) were used as input to the simulation along with the particle's size, density, the hole's inner diameter, and experimental flow time $\tau_{exp,flow}$. Simulations were run with a range of viscosities. The viscosities that gave the best fit to the experimental data were determined by comparing the simulated final inner diameter to the experimental final inner diameter of the half-torus geometry. The upper bound and lower bound viscosities were calculated using conservative upper and lower limits to the surface tension, contact angle, and Navier slip length in the simulations (Table S2).

In the experiments where particle cracked after poking, a quarter sphere model with a sharp edge was used as the initial geometry.[103] The viscosity in the simulations was adjusted until the sharp edge moved by 0.5 μm for the observation time of the experiment. A distance of 0.5 μm corresponded to the resolution of the microscope. Since 0.5 μm is an upper limit to the movement in our experiments, the corresponding viscosity extracted from these simulations is considered a lower limit to the true SOA viscosity.

In the poke-flow experiments, we used conditioning times of 20-22 h, 3-19 h, and 1-2 h, for RH values of 47-67%, 70-89%, and 90-97%, respectively. For RH values of 70-97%, the mixing time of water in the particles was shorter than the conditioning times, indicating the particles reached near-equilibrium conditions with the surrounding RH prior to poking (Section S4 and Table S3). For RH values of 47-60% the mixing times of water within the particles was longer than the conditioning times (Section S3 and Table S3). Under these conditions, however, poking the particles caused them to crack. Continuing the conditioning process will most likely result in the same type of cracking, and we can expect the same viscosity outcome because additional conditioning, which involves further drying, tends to increase viscosity.

When conditioning the SOA particles, the particles were exposed to a flow of ~1 L min^{-1}. A set of separate experiments show that evaporation of semi-volatile organic compounds was small, if any during conditioning (Section S4 and Figs. S4 and S7).

3. Results and Discussion

3.1. Hygroscopicity of Guaiacol SOA

Mass-based hygroscopic growth factors (mass growth factors), the ratio of the particle mass at a certain RH to the particle mass under dry conditions (RH < 1%), were determined with a quartz crystal microbalance for both guaiacol-NO_3 and guaiacol-OH SOA (Fig. 3a). The mass-based hygroscopic growth factor for guaiacol-NO_3 SOA particles was 1.01-1.05 at RH ≤ 80%. The guaiacol-OH SOA hygroscopic growth factor was 1.03-1.25, significantly higher over the same RH range. Above 95% RH, the hygroscopic growth factor for guaiacol-NO_3 SOA drastically increased. This drastic increase may have been due to liquid-liquid phase separation occurring within the SOA at RH values above 95%. Previous thermodynamic calculations have shown that a low-polarity SOA can exist as an organic-rich phase below approximately 95% and undergo liquid-liquid phase separation at high RH values to form an organic-rich and water-rich phase, concurrent with a drastic increase in the SOA hygroscopic growth factor.[101,105,106]

Mass-based hygroscopicity parameters (k_m, Eq. 1) were also determined with QCM measurements (Fig. 3b). Guaiacol-OH SOA has k_m values of 0.085 to 0.136 at ≤ 80% RH. Guaiacol-NO_3 SOA has k_m values of 0.006 to 0.024, significantly lower under the same RH range. The significantly

lower k_m values for guaiacol-NO_3 SOA is consistent with previous studies. For example, Suda et al. showed that the hygroscopicity parameter is lower for organic molecules with NO_3-functional groups compared to carboxylic acid, peroxide, and alcohol functional groups.[107] In addition, Zhang et al. showed that the hygroscopicity parameter for SOA generated by NO_3 oxidation of monoterpenes was much reduced compared to SOA generated by OH and O_3 oxidation of monoterpenes.[89]

3.2. Room Temperature Viscosity as a Function of RH

The poke-flow technique was used to determine the viscosity of the guaiacol-NO_3 SOA at 294 K as a function of RH. At $\lesssim$ 60% RH, the particles cracked and did not flow for up to 21 h (e.g. Fig. 2, 1st row), indicating high viscosity and likely glassy phase state. At $\gtrsim$ 70% RH, the particles flowed when poked (e.g. Fig 2, 2nd and 3nd row). Cracking of SOA particles have been observed previously at room temperature, but only at $\lesssim$ 25% RH.[65,108–112]

A summary of the experimental flow times determined with the poke-flow technique for guaiacol-NO_3 SOA are shown in Fig. S8. The corresponding viscosities are shown in Fig. 4, with viscosity measurements at similar RH values combined to determine overall upper and lower limits. The viscosity of guaiacol-NO_3 SOA is high ($\gtrsim 5\times10^7$ Pa s) at RH values $\lesssim$ 70%. For reference, the viscosity of tar pitch is ~10^8 Pa s. Even at 80% RH, the viscosity of guaiacol-NO_3 is still ~ 6×10^5 Pa s. Our results are consistent with previous studies that suggested SOA generated with NO_3 may be highly viscous.[64,67]

For comparison purposes, in Fig. 4a we have included the viscosities of guaiacol-OH SOA reported by Kiland et al.[65] The viscosity of guaiacol-NO_3 SOA is significantly higher than guaiacol-0H SOA at $\gtrsim$ 20% RH (Fig. 4a). For instance, at 40-50% RH, the viscosity of guaiacol-NO_3 SOA particles is > 5 orders of magnitude higher than that of guaiacol-0H SOA particles. These results emphasize that phenolic SOA produced at night could be much more viscous than phenolic SOA produced during the day.

The difference between the viscosities of guaiacol-NO_3 SOA and guaiacol-OH SOA at $\gtrsim$ 20% RH can be explained, at least in part, by a lower hygroscopicity parameter for guaiacol-NO_3 SOA

compared to guaiacol-OH SOA. Water has a very low viscosity (10^{-3} Pa s) and lowers the overall viscosity when added to a high viscosity material, by acting as a plasticizer. A lower hygroscopicity means less water uptake, and hence less reduction in viscosity as relative humidity increases.[78]

Recently, Gregson et al. showed that primary biomass burning organic aerosols generated by smoldering of pine wood contain two phases, a hydrophobic phase and a hydrophilic phase.[113] The viscosity of the hydrophobic phase was largely independent of the RH up to ~95%. The trend we observed for guaiacol-NO_3 SOA is similar to the trend Gregson et al. observed for their hydrophobic phase and can be attributed to the relatively hydrophobic nature of the material.

In Fig. 4b, we have also included the viscosity of other SOA types determined with the poke-flow technique and reported previously.[65,109,112,114,115] All of the other SOA types were generated using OH or O_3 as the oxidant, i.e. major daytime oxidants. The viscosity of guaiacol-NO_3 SOA is drastically higher than the other types of SOA at $\gtrsim$ 40% RH. For example, at 50% RH, the viscosity of guaiacol-NO_3 SOA is 2-6 orders of magnitude higher than that of other SOAs investigated. These results highlight that SOA generated by NO_3 reactions with phenols could be drastically more viscous than other types of SOA. The difference between the viscosities of guaiacol-NO_3 SOA and the other types of SOA can be explained, at least in part, by the low hygroscopicity parameter for guaiacol-NO_3, as discussed above. The differences may also be related to difference in molecular weights of the SOA components. Viscosity is known to correlate with molecular weight,[73,116] and guaiacol-NO_3 SOA contains large molecular weight dimers, based on previous mass spectrometry studies.[7,117]

3.3. Viscosity as a Function of RH and Temperature

To extrapolate the viscosity results for guaiacol-NO_3 shown in Fig. 4a to other RH values and temperatures, we developed parameterizations that can describe the viscosities as a function of both RH and temperature, as done previously (see Section S5).[109,114] For comparison, we have also extrapolated the guaiacol-OH SOA results from Kiland et al.[65] to other RH values and temperatures. First, we fit a mole fraction-based Arrhenius mixing rule to the viscosity data in Fig. 4a, resulting in a parameterization of viscosity as a function of RH at 294 K (dashed lines in Fig. 4a). Second, we extended the 294 K parameterization to higher and lower temperatures using the

Vogel-Fulcher-Tammann equation.[118] Shown in Fig. 5 is the resulting parameterization as a function of both RH and temperature determined using this method. A liquid, semisolid, and amorphous solid phase state (i.e. glassy phase state) have a viscosity of < 10^2 Pa s, 10^2-10^{12} Pa s, and > 10^{12} Pa s, respectively.[78] The viscosity of guaiacol-NO_3 SOA (Fig. 5a) is largely independent of the RH between 0 to 80% at all temperatures. For temperatures less than 270 K and RH lower than 80%, the guaiacol-NO_3 SOA is in a glassy phase state (viscosity > 10^{12} Pa s). In contrast, the guaiacol-OH SOA (Fig. 5b) is strongly dependent on both RH and temperature and only forms a glassy phase state when both the temperature and RH are low.

3.4. Atmospheric Implications

To extrapolate the viscosity results from our study to the atmosphere we combined annual average RH and temperature values in the troposphere with the parameterizations for viscosity as a function of RH and temperature (Fig. 5) following the approach used previously.[109,119] Annual average tropospheric RH and temperature values were extracted from the European Center Hamburg Model/Modular Earth Submodel System Atmospheric Chemistry Model.[120] The results of this extrapolation are presented in Fig. 6 for guaiacol-NO_3 SOA and guaiacol-OH SOA.

Based on our extrapolations (Fig. 6a), guaiacol-NO_3 SOA is most often in a semi-solid state in the planetary boundary layer ($\lesssim$ 1 km in altitude) and a glassy phase state in the free troposphere (1km $\lesssim$ altitude $\lesssim$ 18 km). The liquid state is only predicted for a limited region of the planetary boundary layer ($\gtrsim$ 80 ° latitude). In constant, a liquid state is predicted for almost all conditions in the planetary boundary layer for guaiacol-OH SOA (Fig. 6b). A glassy phase state can limit heterogeneous reactions.[36,41–53] In addition, a glassy phase state can potentially act as a heterogeneous nucleus for ice formation in the atmosphere,[23,58–62] although the importance of the glassy phase state for ice nucleation is still a matter of debate.[64]

Mixing time is defined as the time it takes for the concentration of the diffusing species at the particle's center to deviate by less than 1/e from the equilibrium concentration. Knowledge of the mixing time of organic molecules within SOA particles is important for forecasting both the size distribution and mass of SOA particles.[29–40,69,121,122] Additionally, mixing time plays a key role in

anticipating the long-range transport of pollutants trapped in SOA particles.[54–57,123] Most chemical transport models assume the mixing times of organic molecules is < 1 h.

We calculated the mixing times of organic molecules within guaiacol-NO_3 and guaiacol-OH SOA particles from the viscosity results. The mixing time of organic molecules within the SOA particles ($\tau_{mix,org}$) was calculated based on the following equation:

$$\tau_{mix,org}(RH,T) = \frac{d_p^{\,2}}{4\pi^2\, D_{org}(RH,T)} \qquad \text{Eq. 2}$$

where d_p is the diameter of the SOA particle, assumed to be 200 nm for the troposphere and, $D_{org}(RH,T)$ is the diffusion coefficient of organic molecules within the SOA particle as a function of RH and temperature. The diffusion coefficient of organic molecules within SOA particle was estimated using the Stokes-Einstein equation:

$$D_{org}(RH, T) = \frac{kT}{6\pi\eta(RH, T)R_{diff}} \qquad \text{Eq. 3}$$

where $D_{Org}(RH, T)$ is the RH- and temperature-dependent diffusion coefficient of the organic molecules within SOA, k is the Boltzmann constant, $\eta(RH, T)$ is the RH- and temperature-dependent viscosity of the SOA, and R_{diff} is the radius of the diffusing molecule. For R_{diff}, we assumed a value of 0.4 nm, as done previously, which is generally consistent with the expected sizes of SOA molecules. The Stokes-Einstein equation gives values consistent with experimentally measured diffusion coefficients of organic molecules when the radius of the diffusing molecules is equal to or larger than the radius of the molecules composing the organic matrix.[28,124]

The calculated annual average mixing time of organics within guaiacol-NO_3 and guaiacol-OH SOA particles are shown as a function of latitude and altitude in Fig. 7. For guaiacol-NO_3 SOA (Fig. 7a), mixing times are > 1 h for the vast majority of the troposphere. Mixing times are only < 1 h for some regions of the planetary boundary layer (-70° to -50°, -20° to 20°, and 60° to 90°). In contrast, the mixing times within guaiacol-OH SOA (Fig. 7b) in the planetary boundary layer are always < 1 h. The short mixing times for guaiacol-OH SOA within the planetary boundary layer

are due to the relatively warm temperatures and high RH values in this region of the atmosphere and because the viscosity of guaiacol-OH SOA decreases significantly as RH increases.

Our results suggest that mixing times in phenolic SOA generated from NO_3 may often be > 1 h in the planetary boundary layer and free troposphere. These results have possible implications for predicting the size and mass of biomass burning phenolic SOA and the long-range transport of pollutants within biomass burning phenolic SOA. Additional research is needed to determine if other types of phenolic SOA formed by NO_3 reactions have viscosities and mixing times similar to guaiacol-NO_3 SOA.

The above analysis did not take into account the difference in RH and temperature between day and night. Furthermore, the seasonal differences in RH and temperature in the atmosphere were not considered. Additional studies exploring these aspects would be informative. The lifetime of SOA in the atmosphere is on the order of a few weeks.[22] Hence, SOA generated during the night can affect atmospheric chemistry and air quality during the following day.

The above analysis also did not consider the internal mixing of phenolic-NO_3 SOA with other types of aerosol. Mixing of phenolic-NO_3 SOA with other types of aerosol may lead to lower viscosities than illustrated here if they form a single phase.[125] On the other hand, phenolic-NO_3 SOA may form a separate phase when mixed with other types of aerosols due to differences in polarity and hygroscopicity.[126–129] Studies are needed to determine if phenolic SOA generated by NO_3 reactions will mix with other types of organic aerosol. The particles employed in our study ranged from 50 to 100 μm in diameter. Finite size effects can significantly reduce the viscosities of SOA when the diameter is less than or equal to approximately 100 nm.[130] Consequently, we expect our findings to be relevant to particles larger than approximately 100 nm, but experiments are needed to confirm this hypothesis.

Acknowledgements

We acknowledge the support of the Natural Sciences and Engineering Research Council of Canada (NSERC), [funding reference number RGPIN-2023-05333]. Cette recherche a été financée par le Conseil de recherches en sciences naturelles et en génie du Canada (CRSNG), [numéro de référence RGPIN-2023-05333]. P.L. and B.B. acknowledge the support of National Science Foundation (NSF) under the grant No. AGS-2131458. In addition, we acknowledge ChatGPT 3.5 (Open AI, https://chat.openai.com), which was used to improve the language and grammar of this manuscript.

Figures

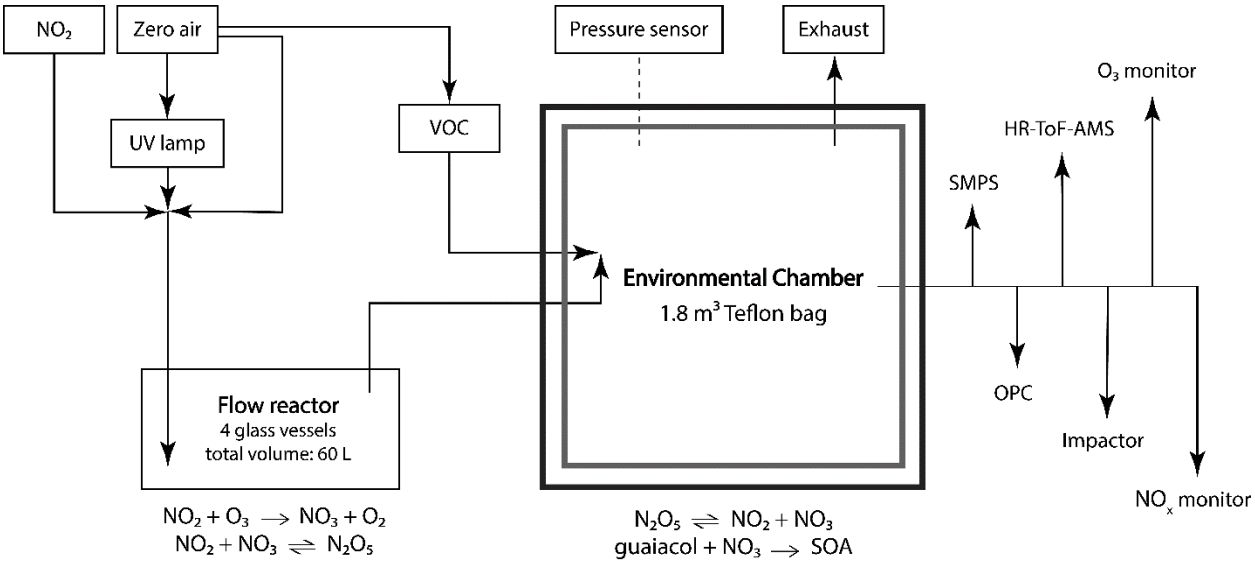

Figure 1. Schematic of the flow reactor and environmental chamber used to generate guaiacol-NO_3 SOA. The high-resolution time-of-flight aerosol mass spectrometer (HR-ToF-AMS), scanning mobility particle sizer (SMPS), and optical particle counter (OPC) were used to monitor the concentration and composition of SOA in the environmental chamber. The O_3 monitor and NO_x monitor were used to monitor the concentration of precursors.

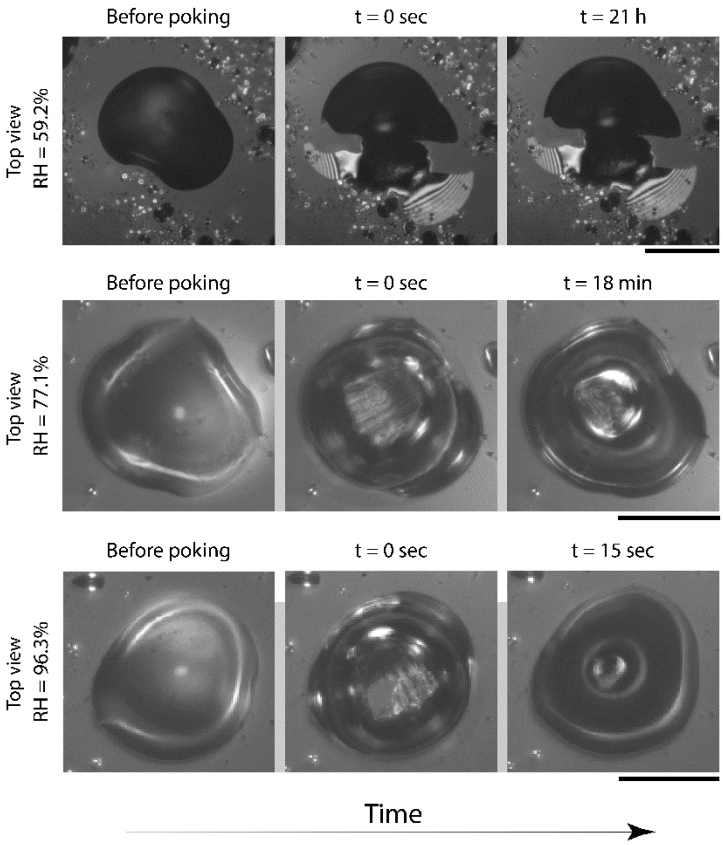

Figure 2. Optical microscope images of SOA particles from guaiacol-NO_3 poked at 59.2%, 77.1%, and 96.3 % RH, captured with the poke-flow setup. The scale bars represent 50 µm.

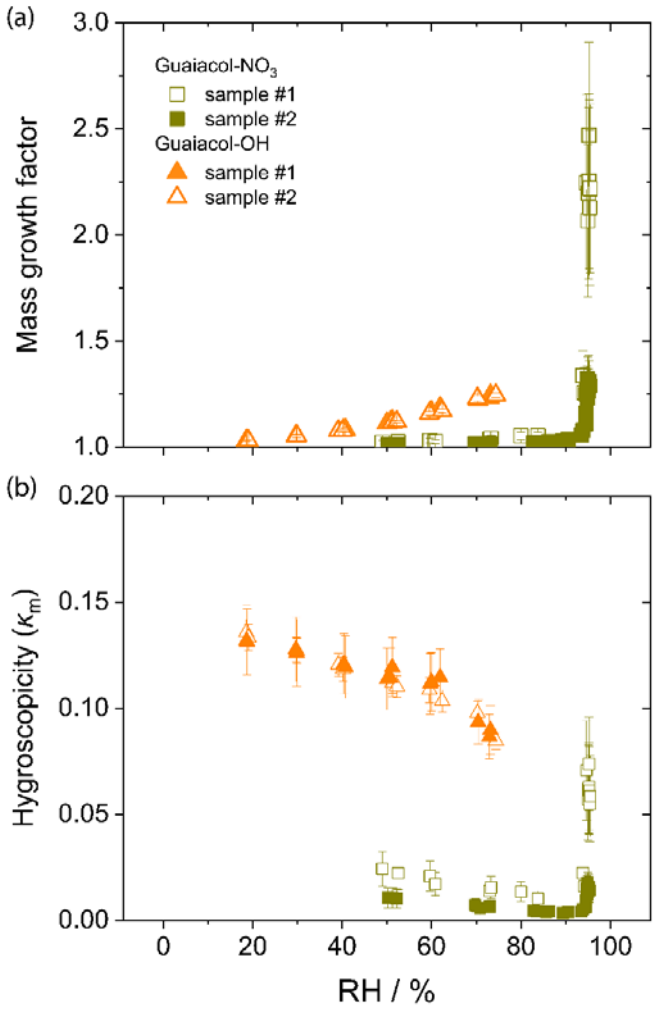

Figure 3. (a) Mass hygroscopic growth factor results from QCM measurements for guaiacol-OH and guaiacol-NO_3 SOA particles as a function of RH. (b) Mass-based hygroscopicity parameter (k_m) for guaiacol-OH and guaiacol-NO_3 SOA particles under different RH values.

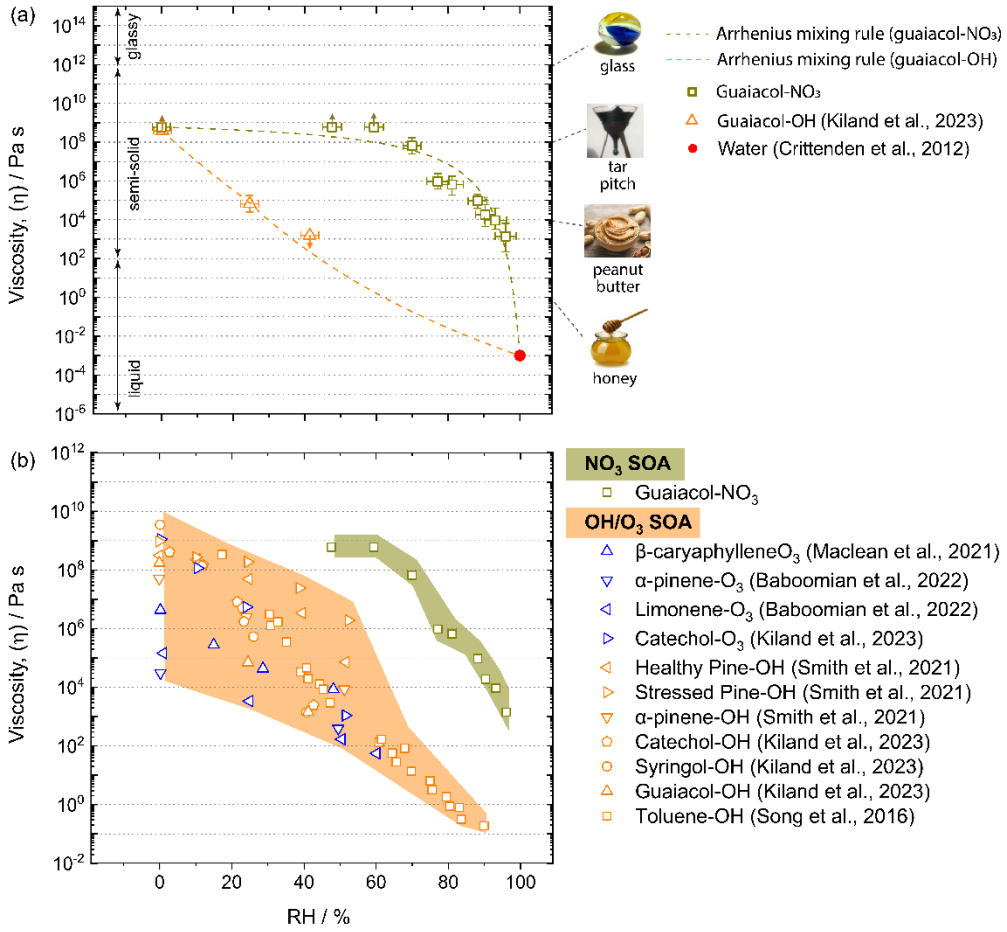

Figure 4. Results from the poke-flow experiments. (a) The viscosity for guaiacol-NO_3 SOA (green squares) and guaiacol-OH SOA (orange triangles). The higher and lower limits of viscosities measured from the poke-flow experiments for repeat runs of the same SOA and RH conditions are shown as y-error bars and the symbols represent the midpoint on a log scale. The x-error bars represent the uncertainty in RH. The red filled circle represents the viscosity of pure water at 294 K [131]. The dashed lines show the equation of Arrhenius mixing rule fitted to the viscosity data (see Section S5 for details). The viscosity of guaiacol-NO_3 SOA particle at 0% RH is a lower limit and is based on an extrapolation from the measurements at higher RH values, assuming viscosity does not increase with a decrease in RH. Viscosity data for guaiacol-OH SOA was taken from literature. [65] (b) The viscosity of guaiacol-NO_3 SOA compared to other SOAs oxidized with OH/O_3 and measured with the poke-flow technique. Each data point represents the average value and error bars have been omitted for clarity. The green and orange bands are added to aid in distinguishing the viscosity difference between NO_3 and OH/O_3 SOAs, respectively.

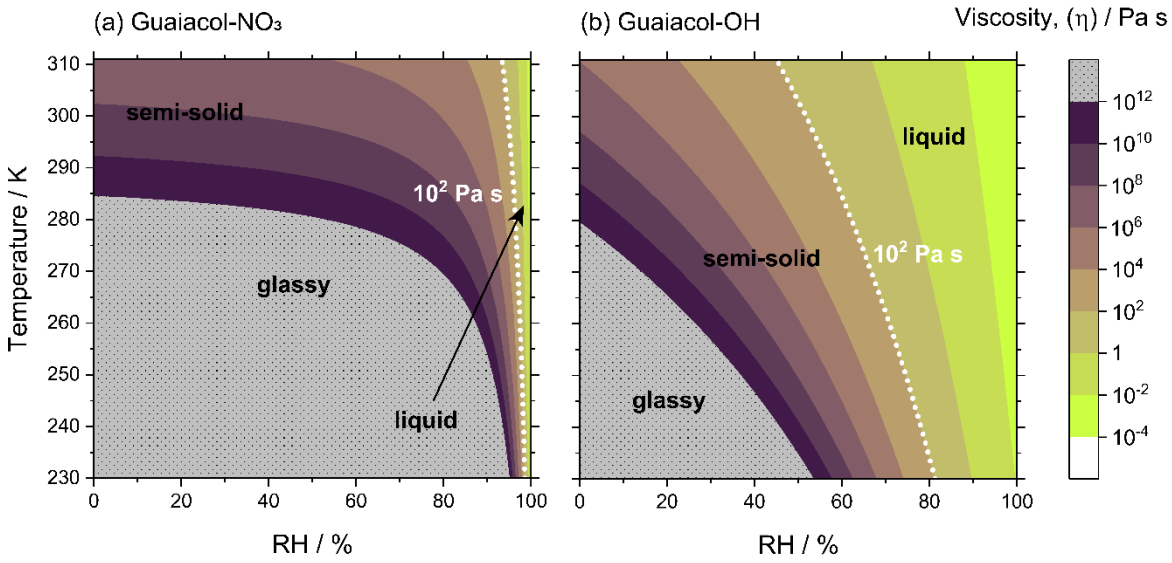

Figure 5. The viscosity of (a) guaiacol-NO_3 SOA and (b) guaiacol-OH SOA as a function of RH and temperature. The white dotted line represents the transition from liquid to semi-solid, which occurs at a viscosity of 10^2 Pa s. The glassy phase state is shown with grey color where viscosity is 10^{12} Pa s or higher.

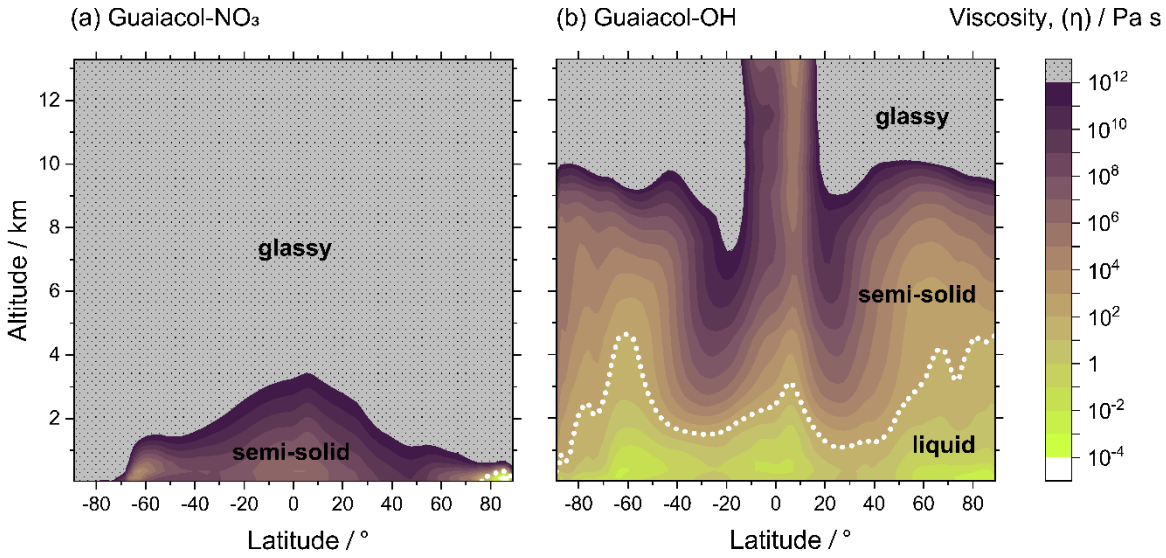

Figure 6. The zonally averaged viscosity of (a) guaiacol-NO_3 SOA and (b) guaiacol-OH SOA particles as a function of latitude and altitude in the troposphere. The white dotted line represents the transition from liquid to semi-solid phase.

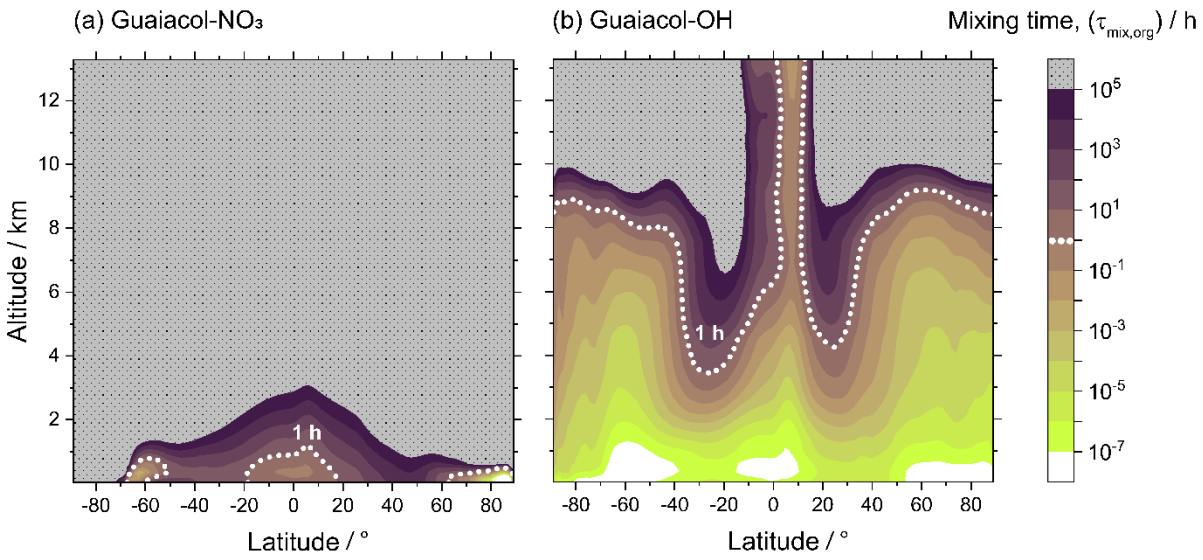

Figure 7. Annually averaged mixing times of organic molecules within 200 nm SOA particles: (a) guaiacol-NO_3 and (b) guaiacol-OH SOA particles. The white dotted line highlights the mixing times of 1 h. Chemical transport models often use the assumption of fast mixing i.e. a mixing time of $\lesssim$ 1 h. Mixing times for the glassy phase state is not shown in this figure.

REFERENCES

(1) Lauraguais, A.; Coeur-Tourneur, C.; Cassez, A.; Deboudt, K.; Fourmentin, M.; Choël, M. Atmospheric Reactivity of Hydroxyl Radicals with Guaiacol (2-Methoxyphenol), a Biomass Burning Emitted Compound: Secondary Organic Aerosol Formation and Gas-Phase Oxidation Products. *Atmos. Environ.* **2014**, *86*, 155–163. https://doi.org/10.1016/j.atmosenv.2013.11.074.

(2) Schauer, J. J.; Kleeman, M. J.; Cass, G. R.; Simoneit, B. R. T. Measurement of Emissions from Air Pollution Sources. 3. C1-C29 Organic Compounds from Fireplace Combustion of Wood. *Environ. Sci. Technol.* **2001**, *35* (9), 1716–1728. https://doi.org/10.1021/es001331e.

(3) Yang, B.; Zhang, H.; Wang, Y.; Zhang, P.; Shu, J.; Sun, W.; Ma, P. Experimental and Theoretical Studies on Gas-Phase Reactions of NO3 Radicals with Three Methoxyphenols: Guaiacol, Creosol, and Syringol. *Atmos. Environ.* **2016**, *125* (3), 243–251. https://doi.org/10.1016/j.atmosenv.2015.11.028.

(4) Hatch, L. E.; Luo, W.; Pankow, J. F.; Yokelson, R. J.; Stockwell, C. E.; Barsanti, K. C. Identification and Quantification of Gaseous Organic Compounds Emitted from Biomass Burning Using Two-Dimensional Gas Chromatography-Time-of-Flight Mass Spectrometry. *Atmos. Chem. Phys.* **2015**, *15* (4), 1865–1899. https://doi.org/10.5194/acp-15-1865-2015.

(5) Yee, L. D.; Kautzman, K. E.; Loza, C. L.; Schilling, K. A.; Coggon, M. M.; Chhabra, P. S.; Chan, M. N.; Chan, A. W. H.; Hersey, S. P.; Crounse, J. D.; Wennberg, P. O.; Flagan, R. C.; Seinfeld, J. H. Secondary Organic Aerosol Formation from Biomass Burning Intermediates: Phenol and Methoxyphenols. *Atmos. Chem. Phys.* **2013**, *13* (16), 8019–8043. https://doi.org/10.5194/acp-13-8019-2013.

(6) Liang, Y.; Jen, C. N.; Weber, R. J.; Misztal, P. K.; Goldstein, A. H. Chemical Composition of PM2.5 in October 2017 Northern California Wildfire Plumes. *Atmos. Chem. Phys.* **2021**, *21* (7), 5719–5737. https://doi.org/10.5194/acp-21-5719-2021.

(7) Mayorga, R. J.; Zhao, Z.; Zhang, H. Formation of Secondary Organic Aerosol from Nitrate Radical Oxidation of Phenolic VOCs: Implications for Nitration Mechanisms and Brown Carbon Formation. *Atmos. Environ.* **2021**, *244* (September 2020), 117910. https://doi.org/10.1016/j.atmosenv.2020.117910.

(8) Ramasamy, S.; Nakayama, T.; Imamura, T.; Morino, Y.; Kajii, Y.; Sato, K. Investigation of Dark Condition Nitrate Radical- and Ozone-Initiated Aging of Toluene Secondary Organic Aerosol: Importance of Nitrate Radical Reactions with Phenolic Products. *Atmos. Environ.* **2019**, *219* (July), 117049. https://doi.org/10.1016/j.atmosenv.2019.117049.

(9) Finewax, Z.; De Gouw, J. A.; Ziemann, P. J. Products and Secondary Organic Aerosol Yields from the OH and NO3 Radical-Initiated Oxidation of Resorcinol. *ACS Earth Sp. Chem.* **2019**, *3* (7), 1248–1259. https://doi.org/10.1021/acsearthspacechem.9b00112.

(10) Sekimoto, K.; Koss, A. R.; Gilman, J. B.; Selimovic, V.; Coggon, M. M.; Zarzana, K. J.;

Yuan, B.; Lerner, B. M.; Brown, S. S.; Warneke, C.; Yokelson, R. J.; Roberts, J. M.; De Gouw, J. High-and Low-Temperature Pyrolysis Profiles Describe Volatile Organic Compound Emissions from Western US Wildfire Fuels. *Atmos. Chem. Phys.* **2018**, *18* (13), 9263–9281. https://doi.org/10.5194/acp-18-9263-2018.

(11) Yee, L. D.; Kautzman, K. E.; Loza, C. L.; Schilling, K. A.; Coggon, M. M.; Chhabra, P. S.; Chan, M. N.; Chan, A. W. H.; Hersey, S. P.; Crounse, J. D.; Wennberg, P. O.; Flagan, R. C.; Seinfeld, J. H. Secondary Organic Aerosol Formation from Biomass Burning Intermediates: Phenol and Methoxyphenols. *Atmos. Chem. Phys.* **2013**, *13* (16), 8019–8043. https://doi.org/10.5194/acp-13-8019-2013.

(12) Finewax, Z.; De Gouw, J. A.; Ziemann, P. J. Identification and Quantification of 4-Nitrocatechol Formed from OH and NO3 Radical-Initiated Reactions of Catechol in Air in the Presence of NOx: Implications for Secondary Organic Aerosol Formation from Biomass Burning. *Environ. Sci. Technol.* **2018**, *52* (4), 1981–1989. https://doi.org/10.1021/acs.est.7b05864.

(13) Lauraguais, A.; Coeur-Tourneur, C.; Cassez, A.; Seydi, A. Rate Constant and Secondary Organic Aerosol Yields for the Gas-Phase Reaction of Hydroxyl Radicals with Syringol (2,6-Dimethoxyphenol). *Atmos. Environ.* **2012**, *55*, 43–48. https://doi.org/10.1016/j.atmosenv.2012.02.027.

(14) Lauraguais, A.; Coeur-Tourneur, C.; Cassez, A.; Deboudt, K.; Fourmentin, M.; Choël, M. Atmospheric Reactivity of Hydroxyl Radicals with Guaiacol (2-Methoxyphenol), a Biomass Burning Emitted Compound: Secondary Organic Aerosol Formation and Gas-Phase Oxidation Products. *Atmos. Environ.* **2014**, *86*, 155–163. https://doi.org/10.1016/j.atmosenv.2013.11.074.

(15) Coeur-Tourneur, C.; Tomas, A.; Guilloteau, A.; Henry, F.; Ledoux, F.; Visez, N.; Riffault, V.; Wenger, J. C.; Bedjanian, Y. Aerosol Formation Yields from the Reaction of Catechol with Ozone. *Atmos. Environ.* **2009**, *43* (14), 2360–2365. https://doi.org/10.1016/j.atmosenv.2008.12.054.

(16) Decker, Z. C. J.; Robinson, M. A.; Barsanti, K. C.; Bourgeois, I.; Coggon, M. M.; Digangi, J. P.; Diskin, G. S.; Flocke, F. M.; Franchin, A.; Fredrickson, C. D.; Gkatzelis, G. I.; Hall, S. R.; Halliday, H.; Holmes, C. D.; Huey, L. G.; Lee, Y. R.; Lindaas, J.; Middlebrook, A. M.; Montzka, D. D.; Moore, R.; Neuman, J. A.; Nowak, J. B.; Palm, B. B.; Peischl, J.; Piel, F.; Rickly, P. S.; Rollins, A. W.; Ryerson, T. B.; Schwantes, R. H.; Sekimoto, K.; Thornhill, L.; Thornton, J. A.; Tyndall, G. S.; Ullmann, K.; Van Rooy, P.; Veres, P. R.; Warneke, C.; Washenfelder, R. A.; Weinheimer, A. J.; Wiggins, E.; Winstead, E.; Wisthaler, A.; Womack, C.; Brown, S. S. Nighttime and Daytime Dark Oxidation Chemistry in Wildfire Plumes: An Observation and Model Analysis of FIREX-AQ Aircraft Data. *Atmos. Chem. Phys.* **2021**, *21* (21), 16293–16317. https://doi.org/10.5194/acp-21-16293-2021.

(17) Akherati, A.; He, Y.; Coggon, M. M.; Koss, A. R.; Hodshire, A. L.; Sekimoto, K.; Warneke, C.; De Gouw, J.; Yee, L.; Seinfeld, J. H.; Onasch, T. B.; Herndon, S. C.; Knighton, W. B.; Cappa, C. D.; Kleeman, M. J.; Lim, C. Y.; Kroll, J. H.; Pierce, J. R.; Jathar, S. H. Oxygenated Aromatic Compounds Are Important Precursors of Secondary Organic Aerosol

in Biomass-Burning Emissions. *Environ. Sci. Technol.* **2020**, *54* (14), 8568–8579. https://doi.org/10.1021/acs.est.0c01345.

(18) Finlayson-Pitts, B. J.; Pitts Jr, J. N. *Chemistry of the Upper and Lower Atmosphere: Theory, Experiments, and Applications*; Elsevier, 1999.

(19) Kodros, J. K.; Papanastasiou, D. K.; Paglione, M.; Masiol, M.; Squizzato, S.; Florou, K.; Skyllakou, K.; Kaltsonoudis, C.; Nenes, A.; Pandis, S. N. Rapid Dark Aging of Biomass Burning as an Overlooked Source of Oxidized Organic Aerosol. *Proc. Natl. Acad. Sci. U. S. A.* **2020**, *117* (52), 33028–33033. https://doi.org/10.1073/PNAS.2010365117.

(20) Shrivastava, M.; Cappa, C. D.; Fan, J.; Goldstein, A. H.; Guenther, A. B.; Jimenez, J. L.; Kuang, C.; Laskin, A.; Martin, S. T.; Ng, N. L.; Petaja, T.; Pierce, J. R.; Rasch, P. J.; Roldin, P.; Seinfeld, J. H.; Shilling, J.; Smith, J. N.; Thornton, J. A.; Volkamer, R.; Wang, J.; Worsnop, D. R.; Zaveri, R. A.; Zelenyuk, A.; Zhang, Q. Recent Advances in Understanding Secondary Organic Aerosol: Implications for Global Climate Forcing. *Rev. Geophys.* **2017**, *55* (2), 509–559. https://doi.org/10.1002/2016RG000540.

(21) Hallquist, M.; Wenger, J. C.; Baltensperger, U.; Rudich, Y.; Simpson, D.; Claeys, M.; Dommen, J.; Donahue, N. M.; George, C.; Goldstein, A. H.; Hamilton, J. F.; Herrmann, H.; Hoffmann, T.; Iinuma, Y.; Jang, M.; Jenkin, M. E.; Jimenez, J. L.; Kiendler-Scharr, A.; Maenhaut, W.; McFiggans, G.; Mentel, T. F.; Monod, A.; Prévôt, A. S. H.; Seinfeld, J. H.; Surratt, J. D.; Szmigielski, R.; Wildt, J. The Formation, Properties and Impact of Secondary Organic Aerosol: Current and Emerging Issues. *Atmos. Chem. Phys.* **2009**, *9* (14), 5155–5236. https://doi.org/10.5194/acp-9-5155-2009.

(22) Tsigaridis, K.; Kanakidou, M. Global Modelling of Secondary Organic Aerosol in the Troposphere: A Sensitivity Analysis. *Atmos. Chem. Phys.* **2003**, *3* (5), 1849–1869. https://doi.org/10.5194/acp-3-1849-2003.

(23) Knopf, D. A.; Alpert, P. A.; Wang, B. The Role of Organic Aerosol in Atmospheric Ice Nucleation: A Review. *ACS Earth Sp. Chem.* **2018**, *2* (3), 168–202. https://doi.org/10.1021/acsearthspacechem.7b00120.

(24) Pope, C. A.; Ezzati, M.; Dockery, D. W. Fine-Particulate Air Pollution and Life Expectancy in the United States. *N. Engl. J. Med.* **2009**, *360* (4), 376–386. https://doi.org/10.1056/nejmsa0805646.

(25) Lighty, J. A. S.; Veranth, J. M.; Sarofim, A. F. Combustion Aerosols: Factors Governing Their Size and Composition and Implications to Human Health. *J. Air Waste Manag. Assoc.* **2000**, *50* (9), 1565–1618. https://doi.org/10.1080/10473289.2000.10464197.

(26) Lelieveld, J.; Evans, J. S.; Fnais, M.; Giannadaki, D.; Pozzer, A. The Contribution of Outdoor Air Pollution Sources to Premature Mortality on a Global Scale. *Nature* **2015**, *525* (7569), 367–371. https://doi.org/10.1038/nature15371.

(27) Reid, J. P.; Bertram, A. K.; Topping, D. O.; Laskin, A.; Martin, S. T.; Petters, M. D.; Pope, F. D.; Rovelli, G. The Viscosity of Atmospherically Relevant Organic Particles. *Nat. Commun.* **2018**, *9* (1), 1–14. https://doi.org/10.1038/s41467-018-03027-z.

(28) Evoy, E.; Kamal, S.; Patey, G. N.; Martin, S. T.; Bertram, A. K. Unified Description of Diffusion Coefficients from Small to Large Molecules in Organic-Water Mixtures. *J. Phys. Chem. A* **2020**, *124* (11), 2301–2308. https://doi.org/10.1021/acs.jpca.9b11271.

(29) Kim, Y.; Sartelet, K.; Couvidat, F. Modeling the Effect of Non-Ideality, Dynamic Mass Transfer and Viscosity on SOA Formation in a 3-D Air Quality Model. *Atmos. Chem. Phys.* **2019**, *19* (2), 1241–1261. https://doi.org/10.5194/acp-19-1241-2019.

(30) Zaveri, R. A.; Shilling, J. E.; Zelenyuk, A.; Liu, J.; Bell, D. M.; D'Ambro, E. L.; Gaston, C. J.; Thornton, J. A.; Laskin, A.; Lin, P.; Wilson, J.; Easter, R. C.; Wang, J.; Bertram, A. K.; Martin, S. T.; Seinfeld, J. H.; Worsnop, D. R. Growth Kinetics and Size Distribution Dynamics of Viscous Secondary Organic Aerosol. *Environ. Sci. Technol.* **2018**, *52* (3), 1191–1199. https://doi.org/10.1021/acs.est.7b04623.

(31) Vander Wall, A. C.; Perraud, V.; Wingen, L. M.; Finlayson-Pitts, B. J. Evidence for a Kinetically Controlled Burying Mechanism for Growth of High Viscosity Secondary Organic Aerosol. *Environ. Sci. Process. Impacts* **2020**, *22* (1), 66–83. https://doi.org/10.1039/c9em00379g.

(32) Zaveri, R. A.; Wang, J.; Fan, J.; Zhang, Y.; Shilling, J. E.; Zelenyuk, A.; Mei, F.; Newsom, R.; Pekour, M.; Tomlinson, J.; Comstock, J. M.; Shrivastava, M.; Fortner, E.; Machado, L. A. T.; Artaxo, P.; Martin, S. T. Rapid Growth of Anthropogenic Organic Nanoparticles Greatly Alters Cloud Life Cycle in the Amazon Rainforest. *Sci. Adv.* **2022**, *8* (2), 1–17. https://doi.org/10.1126/sciadv.abj0329.

(33) Ye, J.; Van Rooy, P.; Adam, C. H.; Jeong, C. H.; Urch, B.; Cocker, D. R.; Evans, G. J.; Chan, A. W. H. Predicting Secondary Organic Aerosol Enhancement in the Presence of Atmospherically Relevant Organic Particles. *ACS Earth Sp. Chem.* **2018**, *2* (10), 1035–1046. https://doi.org/10.1021/acsearthspacechem.8b00093.

(34) Zaveri, R. A.; Easter, R. C.; Shilling, J. E.; Seinfeld, J. H. Modeling Kinetic Partitioning of Secondary Organic Aerosol and Size Distribution Dynamics: Representing Effects of Volatility, Phase State, and Particle-Phase Reaction. *Atmos. Chem. Phys.* **2014**, *14* (10), 5153–5181. https://doi.org/10.5194/acp-14-5153-2014.

(35) Shiraiwa, M.; Seinfeld, J. H. Equilibration Timescale of Atmospheric Secondary Organic Aerosol Partitioning. *Geophys. Res. Lett.* **2012**, *39* (24), 1–6. https://doi.org/10.1029/2012GL054008.

(36) Shiraiwa, M.; Ammann, M.; Koop, T.; Pöschl, U. Gas Uptake and Chemical Aging of Semisolid Organic Aerosol Particles. *Proc. Natl. Acad. Sci. U. S. A.* **2011**, *108* (27), 11003–11008. https://doi.org/10.1073/pnas.1103045108.

(37) Shiraiwa, M.; Yee, L. D.; Schilling, K. A.; Loza, C. L.; Craven, J. S.; Zuend, A.; Ziemann, P. J.; Seinfeld, J. H. Size Distribution Dynamics Reveal Particle-Phase Chemistry in Organic Aerosol Formation. *Proc. Natl. Acad. Sci. U. S. A.* **2013**, *110* (29), 11746–11750. https://doi.org/10.1073/pnas.1307501110.

(38) Yli-Juuti, T.; Pajunoja, A.; Tikkanen, O. P.; Buchholz, A.; Faiola, C.; Väisänen, O.; Hao,

L.; Kari, E.; Peräkylä, O.; Garmash, O.; Shiraiwa, M.; Ehn, M.; Lehtinen, K.; Virtanen, A. Factors Controlling the Evaporation of Secondary Organic Aerosol from α-Pinene Ozonolysis. *Geophys. Res. Lett.* **2017**, *44* (5), 2562–2570. https://doi.org/10.1002/2016GL072364.

(39) Zhang, Y.; Chen, Y.; Lei, Z.; Olson, N. E.; Riva, M.; Koss, A. R.; Zhang, Z.; Gold, A.; Jayne, J. T.; Worsnop, D. R.; Onasch, T. B.; Kroll, J. H.; Turpin, B. J.; Ault, A. P.; Surratt, J. D. Joint Impacts of Acidity and Viscosity on the Formation of Secondary Organic Aerosol from Isoprene Epoxydiols (IEPOX) in Phase Separated Particles. *ACS Earth Sp. Chem.* **2019**, *3* (12), 2646–2658. https://doi.org/10.1021/acsearthspacechem.9b00209.

(40) Han, Y.; Gong, Z.; Ye, J.; Liu, P.; McKinney, K. A.; Martin, S. T. Quantifying the Role of the Relative Humidity-Dependent Physical State of Organic Particulate Matter in the Uptake of Semivolatile Organic Molecules. *Environ. Sci. Technol.* **2019**. https://doi.org/10.1021/acs.est.9b05354.

(41) Shrivastava, M.; Lou, S.; Zelenyuk, A.; Easter, R. C.; Corley, R. A.; Thrall, B. D.; Rasch, P. J.; Fast, J. D.; Massey Simonich, S. L.; Shen, H.; Tao, S. Global Long-Range Transport and Lung Cancer Risk from Polycyclic Aromatic Hydrocarbons Shielded by Coatings of Organic Aerosol. *Proc. Natl. Acad. Sci. U. S. A.* **2017**, *114* (6), 1246–1251. https://doi.org/10.1073/pnas.1618475114.

(42) Shen, C.; Zhang, W.; Choczynski, J.; Davies, J. F.; Zhang, H. Phase State and Relative Humidity Regulate the Heterogeneous Oxidation Kinetics and Pathways of Organic-Inorganic Mixed Aerosols. *Environ. Sci. Technol.* **2022**, *56* (22), 15398–15407. https://doi.org/10.1021/acs.est.2c04670.

(43) Alpert, P. A.; Dou, J.; Corral Arroyo, P.; Schneider, F.; Xto, J.; Luo, B.; Peter, T.; Huthwelker, T.; Borca, C. N.; Henzler, K. D.; Schaefer, T.; Herrmann, H.; Raabe, J.; Watts, B.; Krieger, U. K.; Ammann, M. Photolytic Radical Persistence Due to Anoxia in Viscous Aerosol Particles. *Nat. Commun.* **2021**, *12* (1), 1–8. https://doi.org/10.1038/s41467-021-21913-x.

(44) Dalton, A. B.; Nizkorodov, S. A. Photochemical Degradation of 4-Nitrocatechol and 2,4-Dinitrophenol in a Sugar-Glass Secondary Organic Aerosol Surrogate. *Environ. Sci. Technol.* **2021**, *55* (21), 14586–14594. https://doi.org/10.1021/acs.est.1c04975.

(45) Kuwata, M.; Martin, S. T. Phase of Atmospheric Secondary Organic Material Affects Its Reactivity. *Proc. Natl. Acad. Sci. U. S. A.* **2012**, *109* (43), 17354–17359. https://doi.org/10.1073/pnas.1209071109.

(46) Schmedding, R.; Rasool, Q. Z.; Zhang, Y.; Pye, H. O. T.; Zhang, H.; Chen, Y.; Surratt, J. D.; Lopez-Hilfiker, F. D.; Thornton, J. A.; Goldstein, A. H.; Vizuete, W. Predicting Secondary Organic Aerosol Phase State and Viscosity and Its Effect on Multiphase Chemistry in a Regional-Scale Air Quality Model. *Atmos. Chem. Phys.* **2020**, *20* (13), 8201–8225. https://doi.org/10.5194/acp-20-8201-2020.

(47) Gržinić, G.; Bartels-Rausch, T.; Berkemeier, T.; Türler, A.; Ammann, M. Viscosity Controls Humidity Dependence of N2O5 Uptake to Citric Acid Aerosol. *Atmos. Chem.*

Phys. **2015**, *15* (23), 13615–13625. https://doi.org/10.5194/acp-15-13615-2015.

(48) Marshall, F. H.; Miles, R. E. H.; Song, Y. C.; Ohm, P. B.; Power, R. M.; Reid, J. P.; Dutcher, C. S. Diffusion and Reactivity in Ultraviscous Aerosol and the Correlation with Particle Viscosity. *Chem. Sci.* **2016**, *7* (2), 1298–1308. https://doi.org/10.1039/c5sc03223g.

(49) Steimer, S. S.; Lampimäki, M.; Coz, E.; Grzinic, G.; Ammann, M. The Influence of Physical State on Shikimic Acid Ozonolysis: A Case for in Situ Microspectroscopy. *Atmos. Chem. Phys.* **2014**, *14* (19), 10761–10772. https://doi.org/10.5194/acp-14-10761-2014.

(50) Li, J.; Knopf, D. A. Representation of Multiphase OH Oxidation of Amorphous Organic Aerosol for Tropospheric Conditions. *Environ. Sci. Technol.* **2021**, *55* (11), 7266–7275. https://doi.org/10.1021/acs.est.0c07668.

(51) Li, W.; Teng, X.; Chen, X.; Liu, L.; Xu, L.; Zhang, J.; Wang, Y.; Zhang, Y.; Shi, Z. Organic Coating Reduces Hygroscopic Growth of Phase-Separated Aerosol Particles. *Environ. Sci. Technol.* **2021**, *55* (24), 16339–16346. https://doi.org/10.1021/acs.est.1c05901.

(52) Liu, P.; Li, Y. J.; Wang, Y.; Bateman, A. P.; Zhang, Y.; Gong, Z.; Bertram, A. K.; Martin, S. T. Highly Viscous States Affect the Browning of Atmospheric Organic Particulate Matter. *ACS Cent. Sci.* **2018**, *4* (2), 207–215. https://doi.org/10.1021/acscentsci.7b00452.

(53) Zhang, Y.; Chen, Y.; Lambe, A. T.; Olson, N. E.; Lei, Z.; Craig, R. L.; Zhang, Z.; Gold, A.; Onasch, T. B.; Jayne, J. T.; Worsnop, D. R.; Gaston, C. J.; Thornton, J. A.; Vizuete, W.; Ault, A. P.; Surratt, J. D. Effect of the Aerosol-Phase State on Secondary Organic Aerosol Formation from the Reactive Uptake of Isoprene-Derived Epoxydiols (IEPOX). *Environ. Sci. Technol. Lett.* **2018**, *5* (3), 167–174. https://doi.org/10.1021/acs.estlett.8b00044.

(54) Zelenyuk, A.; Imre, D.; Beránek, J.; Abramson, E.; Wilson, J.; Shrivastava, M. Synergy between Secondary Organic Aerosols and Long-Range Transport of Polycyclic Aromatic Hydrocarbons. *Environ. Sci. Technol.* **2012**, *46* (22), 12459–12466. https://doi.org/10.1021/es302743z.

(55) Friedman, C. L.; Pierce, J. R.; Selin, N. E. Assessing the Influence of Secondary Organic versus Primary Carbonaceous Aerosols on Long-Range Atmospheric Polycyclic Aromatic Hydrocarbon Transport. *Environ. Sci. Technol.* **2014**, *48* (6), 3293–3302. https://doi.org/10.1021/es405219r.

(56) Mu, Q.; Shiraiwa, M.; Octaviani, M.; Ma, N.; Ding, A.; Su, H.; Lammel, G.; Pöschl, U.; Cheng, Y. Temperature Effect on Phase State and Reactivity Controls Atmospheric Multiphase Chemistry and Transport of PAHs. *Sci. Adv.* **2018**, *4* (3). https://doi.org/10.1126/sciadv.aap7314.

(57) Keyte, I. J.; Harrison, R. M.; Lammel, G. Chemical Reactivity and Long-Range Transport Potential of Polycyclic Aromatic Hydrocarbons-a Review. *Chem. Soc. Rev.* **2013**, *42* (24), 9333–9391. https://doi.org/10.1039/c3cs60147a.

(58) Murray, B. J.; Wilson, T. W.; Dobbie, S.; Cui, Z.; Al-Jumur, S. M. R. K.; Möhler, O.; Schnaiter, M.; Wagner, R.; Benz, S.; Niemand, M.; Saathoff, H.; Ebert, V.; Wagner, S.;

Kärcher, B. Heterogeneous Nucleation of Ice Particles on Glassy Aerosols under Cirrus Conditions. *Nat. Geosci.* **2010**, *3* (4), 233–237. https://doi.org/10.1038/ngeo817.

(59) Wilson, T. W.; Murray, B. J.; Wagner, R.; Möhler, O.; Saathoff, H.; Schnaiter, M.; Skrotzki, J.; Price, H. C.; Malkin, T. L.; Dobbie, S.; Al-Jumur, S. M. R. K. Glassy Aerosols with a Range of Compositions Nucleate Ice Heterogeneously at Cirrus Temperatures. *Atmos. Chem. Phys.* **2012**, *12* (18), 8611–8632. https://doi.org/10.5194/acp-12-8611-2012.

(60) Berkemeier, T.; Shiraiwa, M.; Pöschl, U.; Koop, T. Competition between Water Uptake and Ice Nucleation by Glassy Organic Aerosol Particles. *Atmos. Chem. Phys.* **2014**, *14* (22), 12513–12531. https://doi.org/10.5194/acp-14-12513-2014.

(61) Ignatius, K.; Kristensen, T. B.; Järvinen, E.; Nichman, L.; Fuchs, C.; Gordon, H.; Herenz, P.; Hoyle, C. R.; Duplissy, J.; Garimella, S.; Dias, A.; Frege, C.; Höppel, N.; Tröstl, J.; Wagner, R.; Yan, C.; Amorim, A.; Baltensperger, U.; Curtius, J.; Donahue, N. M.; Gallagher, M. W.; Kirkby, J.; Kulmala, M.; Möhler, O.; Saathoff, H.; Schnaiter, M.; Tomé, A.; Virtanen, A.; Worsnop, D.; Stratmann, F. Heterogeneous Ice Nucleation of Viscous Secondary Organic Aerosol Produced from Ozonolysis of α-Pinene. *Atmos. Chem. Phys.* **2016**, *16* (10), 6495–6509. https://doi.org/10.5194/acp-16-6495-2016.

(62) Schill, G. P.; Tolbert, M. A. Heterogeneous Ice Nucleation on Phase-Separated Organic-Sulfate Particles: Effect of Liquid vs. Glassy Coatings. *Atmos. Chem. Phys.* **2013**, *13* (9), 4681–4695. https://doi.org/10.5194/acp-13-4681-2013.

(63) Wolf, M. J.; Zhang, Y.; Zawadowicz, M. A.; Goodell, M.; Froyd, K.; Freney, E.; Sellegri, K.; Rösch, M.; Cui, T.; Winter, M.; Lacher, L.; Axisa, D.; DeMott, P. J.; Levin, E. J. T.; Gute, E.; Abbatt, J.; Koss, A.; Kroll, J. H.; Surratt, J. D.; Cziczo, D. J. A Biogenic Secondary Organic Aerosol Source of Cirrus Ice Nucleating Particles. *Nat. Commun.* **2020**, *11* (1). https://doi.org/10.1038/s41467-020-18424-6.

(64) Kasparoglu, S.; Perkins, R.; Ziemann, P. J.; DeMott, P. J.; Kreidenweis, S. M.; Finewax, Z.; Deming, B. L.; DeVault, M. P.; Petters, M. D. Experimental Determination of the Relationship Between Organic Aerosol Viscosity and Ice Nucleation at Upper Free Tropospheric Conditions. *J. Geophys. Res. Atmos.* **2022**, *127* (16), 1–20. https://doi.org/10.1029/2021JD036296.

(65) Kiland, K. J.; Mahrt, F.; Peng, L.; Nikkho, S.; Zaks, J.; Crescenzo, G. V; Bertram, A. K. Viscosity , Glass Formation , and Mixing Times within Secondary Organic Aerosol from Biomass Burning Phenolics. *ACS Earth Sp. Chem.* **2023**, *7* (7), 1388–1400. https://doi.org/10.1021/acsearthspacechem.3c00039.

(66) Garofalo, L. A.; He, Y.; Jathar, S. H.; Pierce, J. R.; Fredrickson, C. D.; Palm, B. B.; Thornton, J. A.; Mahrt, F.; Crescenzo, G. V.; Bertram, A. K.; Draper, D. C.; Fry, J. L.; Orlando, J.; Zhang, X.; Farmer, D. K. Heterogeneous Nucleation Drives Particle Size Segregation in Sequential Ozone and Nitrate Radical Oxidation of Catechol. *Environ. Sci. Technol.* **2021**, *55* (23), 15637–15645. https://doi.org/10.1021/acs.est.1c02984.

(67) Perraud, V.; Bruns, E. A.; Ezell, M. J.; Johnson, S. N.; Yu, Y.; Alexander, M. L.; Zelenyuk, A.; Imre, D.; Chang, W. L.; Dabdub, D.; Pankow, J. F.; Finlayson-Pitts, B. J.

Nonequilibrium Atmospheric Secondary Organic Aerosol Formation and Growth. *Proc. Natl. Acad. Sci. U. S. A.* **2012**, *109* (8), 2836–2841. https://doi.org/10.1073/pnas.1119909109.

(68) Slade, J. H.; Ault, A. P.; Bui, A. T.; Ditto, J. C.; Lei, Z.; Bondy, A. L.; Olson, N. E.; Cook, R. D.; Desrochers, S. J.; Harvey, R. M.; Erickson, M. H.; Wallace, H. W.; Alvarez, S. L.; Flynn, J. H.; Boor, B. E.; Petrucci, G. A.; Gentner, D. R.; Griffin, R. J.; Shepson, P. B. Bouncier Particles at Night: Biogenic Secondary Organic Aerosol Chemistry and Sulfate Drive Diel Variations in the Aerosol Phase in a Mixed Forest. *Environ. Sci. Technol.* **2019**, *53* (9), 4977–4987. https://doi.org/10.1021/acs.est.8b07319.

(69) Bateman, A. P.; Gong, Z.; Harder, T. H.; De Sá, S. S.; Wang, B.; Castillo, P.; China, S.; Liu, Y.; O'Brien, R. E.; Palm, B. B.; Shiu, H. W.; Cirino, G. G.; Thalman, R.; Adachi, K.; Lizabeth Alexander, M.; Artaxo, P.; Bertram, A. K.; Buseck, P. R.; Gilles, M. K.; Jimenez, J. L.; Laskin, A.; Manzi, A. O.; Sedlacek, A.; Souza, R. A. F.; Wang, J.; Zaveri, R.; Martin, S. T. Anthropogenic Influences on the Physical State of Submicron Particulate Matter over a Tropical Forest. *Atmos. Chem. Phys.* **2017**, *17* (3), 1759–1773. https://doi.org/10.5194/acp-17-1759-2017.

(70) Hallquist, M.; Wenger, J. C.; Baltensperger, U.; Rudich, Y.; Simpson, D.; Claeys, M.; Dommen, J.; Donahue, N. M.; George, C.; Goldstein, A. H.; Hamilton, J. F.; Herrmann, H.; Hoffmann, T.; Iinuma, Y.; Jang, M.; Jenkin, M. E.; Jimenez, J. L.; Kiendler-Scharr, A.; Maenhaut, W.; McFiggans, G.; Mentel, T. F.; Monod, A.; Prevot, A. S. H.; Seinfeld, J. H.; Surratt, J. D.; Szmigielski, R.; Wildt, J. The Formation, Properties and Impact of Secondary Organic Aerosol: Current and Emerging Issues. *Atmos. Chem. Phys.* **2009**, *9* (14), 5155–5236. https://doi.org/10.5194/acp-9-5155-2009.

(71) Kanakidou, M.; Seinfeld, J. H.; Pandis, S. N.; Barnes, I.; Dentener, F. J.; Facchini, M. C.; Van Dingenen, R.; Ervens, B.; Nenes, A.; Nielsen, C. J.; Swietlicki, E.; Putaud, J. P.; Balkanski, Y.; Fuzzi, S.; Horth, J.; Moortgat, G. K.; Winterhalter, R.; Myhre, C. E. L.; Tsigaridis, K.; Vignati, E.; Stephanou, E. G.; Wilson, J. Organic Aerosol and Global Climate Modelling: A Review. *Atmos. Chem. Phys.* **2005**, *5*, 1053–1123. https://doi.org/10.5194/acp-5-1053-2005.

(72) Petters, M. D.; Kreidenweis, S. M. A Single Parameter Representation of Hygroscopic Growth and Cloud Condensation Nucleus Activity-Part 3: Including Surfactant Partitioning. *Atmos. Chem. Phys.* **2013**, *13* (2), 1081–1091. https://doi.org/10.5194/acp-13-1081-2013.

(73) Rothfuss, N. E.; Petters, M. D. Influence of Functional Groups on the Viscosity of Organic Aerosol. *Environ. Sci. Technol.* **2017**, *51* (1), 271–279. https://doi.org/10.1021/acs.est.6b04478.

(74) Bateman, A. P.; Bertram, A. K.; Martin, S. T. Hygroscopic Influence on the Semisolid-to-Liquid Transition of Secondary Organic Materials. *J. Phys. Chem. A* **2015**, *119* (19), 4386–4395. https://doi.org/10.1021/jp508521c.

(75) Mikhailov, E.; Vlasenko, S.; Martin, S. T.; Koop, T.; Pöschl, U. Amorphous and Crystalline Aerosol Particles Interacting with Water Vapor: Conceptual Framework and Experimental Evidence for Restructuring, Phase Transitions and Kinetic Limitations. *Atmos. Chem. Phys.*

2009, *9* (24), 9491–9522. https://doi.org/10.5194/acp-9-9491-2009.

(76) DeRieux, W. S. W.; Li, Y.; Lin, P.; Laskin, J.; Laskin, A.; Bertram, A. K.; Nizkorodov, S. A.; Shiraiwa, M. Predicting the Glass Transition Temperature and Viscosity of Secondary Organic Material Using Molecular Composition. *Atmos. Chem. Phys.* **2018**, *18* (9), 6331–6351. https://doi.org/10.5194/acp-18-6331-2018.

(77) Maclean, A. M.; Smith, N. R.; Li, Y.; Huang, Y.; Hettiyadura, A. P. S.; Crescenzo, G. V; Shiraiwa, M.; Laskin, A.; Nizkorodov, S. A.; Bertram, A. K. Humidity-Dependent Viscosity of Secondary Organic Aerosol from Ozonolysis of β-Caryophyllene: Measurements, Predictions, and Implications. *ACS Earth Sp. Chem.* **2021**, *5* (2), 305–318. https://doi.org/10.1021/acsearthspacechem.0c00296.

(78) Koop, T.; Bookhold, J.; Shiraiwa, M.; Pöschl, U. Glass Transition and Phase State of Organic Compounds: Dependency on Molecular Properties and Implications for Secondary Organic Aerosols in the Atmosphere. *Phys. Chem. Chem. Phys.* **2011**, *13* (43), 19238–19255. https://doi.org/10.1039/c1cp22617g.

(79) Song, M.; Liu, P. F.; Hanna, S. J.; Zaveri, R. A.; Potter, K.; You, Y.; Martin, S. T.; Bertram, A. K. Relative Humidity-Dependent Viscosity of Secondary Organic Material from Toluene Photo-Oxidation and Possible Implications for Organic Particulate Matter over Megacities. *Atmos. Chem. Phys. 16* (14), 8817–8830. https://doi.org/10.5194/acp-16-8817-2016.

(80) Liu, P.; Li, Y. J.; Wang, Y.; Gilles, M. K.; Zaveri, R. A.; Bertram, A. K.; Martin, S. T. Lability of Secondary Organic Particulate Matter. *Proc. Natl. Acad. Sci. U. S. A.* **2016**, *113* (45), 12643–12648. https://doi.org/10.1073/pnas.1603138113.

(81) Varutbangkul, V.; Brechtel, F. J.; Bahreini, R.; Ng, N. L.; Keywood, M. D.; Kroll, J. H.; Flagan, R. C.; Seinfeld, J. H.; Lee, A.; Goldstein, A. H. Hygroscopicity of Secondary Organic Aerosols Formed by Oxidation of Cycloalkenes, Monoterpenes, Sesquiterpenes, and Related Compounds. *Atmos. Chem. Phys.* **2006**, *6* (9), 2367–2388. https://doi.org/10.5194/acp-6-2367-2006.

(82) Duplissy, J.; DeCarlo, P. F.; Dommen, J.; Alfarra, M. R.; Metzger, A.; Barmpadimos, I.; Prevot, A. S. H.; Weingartner, E.; Tritscher, T.; Gysel, M.; Aiken, A. C.; Jimenez, J. L.; Canagaratna, M. R.; Worsnop, D. R.; Collins, D. R.; Tomlinson, J.; Baltensperger, U. Relating Hygroscopicity and Composition of Organic Aerosol Particulate Matter. *Atmos. Chem. Phys.* **2011**, *11* (3), 1155–1165. https://doi.org/10.5194/acp-11-1155-2011.

(83) Lambe, A. T.; Onasch, T. B.; Massoli, P.; Croasdale, D. R.; Wright, J. P.; Ahern, A. T.; Williams, L. R.; Worsnop, D. R.; Brune, W. H.; Davidovits, P. Laboratory Studies of the Chemical Composition and Cloud Condensation Nuclei (CCN) Activity of Secondary Organic Aerosol (SOA) and Oxidized Primary Organic Aerosol (OPOA). *Atmos. Chem. Phys.* **2011**, *11* (17), 8913–8928. https://doi.org/10.5194/acp-11-8913-2011.

(84) Prenni, A. J.; Petters, M. D.; Kreidenweis, S. M.; DeMott, P. J.; Ziemann, P. J. Cloud Droplet Activation of Secondary Organic Aerosol. *J. Geophys. Res. Atmos.* **2007**, *112* (D10). https://doi.org/10.1029/2006jd007963.

(85) Malek, K. A.; Gohil, K.; Al-Abadleh, H. A.; Asa-Awuku, A. A. Hygroscopicity of Polycatechol and Polyguaiacol Secondary Organic Aerosol in Sub- and Supersaturated Water Vapor Environments. *Environ. Sci. Atmos.* **2022**, *2* (1), 24–33. https://doi.org/10.1039/d1ea00063b.

(86) Lei, T.; Zuend, A.; Cheng, Y.; Su, H.; Wang, W.; Ge, M. Hygroscopicity of Organic Surrogate Compounds from Biomass Burning and Their Effect on the Efflorescence of Ammonium Sulfate in Mixed Aerosol Particles. *Atmos. Chem. Phys.* **2018**, *18* (2), 1045–1064. https://doi.org/10.5194/acp-18-1045-2018.

(87) Li, Y. J.; Huang, D. D.; Cheung, H. Y.; Lee, A. K. Y.; Chan, C. K. Aqueous-Phase Photochemical Oxidation and Direct Photolysis of Vanillin - A Model Compound of Methoxy Phenols from Biomass Burning. *Atmos. Chem. Phys.* **2014**, *14* (6), 2871–2885. https://doi.org/10.5194/acp-14-2871-2014.

(88) Betz, K. L.; Calvert, C. T.; Al-Mashala, H. H.; Schnitzler, E. G. Hygroscopicity of Secondary Brown Carbon Aerosol from Aqueous Photo-Oxidation of Phenolic Precursors. *ACS Earth Sp. Chem.* **2022**, *6* (11), 2609–2618. https://doi.org/10.1021/acsearthspacechem.2c00132.

(89) Zhang, C.; Guo, Y.; Shen, H.; Luo, H.; Pullinen, I.; Schmitt, S. H.; Wang, M.; Fuchs, H.; Kiendler-Scharr, A.; Wahner, A.; Mentel, T. F.; Zhao, D. Contrasting Influence of Nitrogen Oxides on the Cloud Condensation Nuclei Activity of Monoterpene-Derived Secondary Organic Aerosol in Daytime and Nighttime Oxidation. *Geophys. Res. Lett.* **2023**, *50* (4). https://doi.org/10.1029/2022gl102110.

(90) Kuang, Y.; Xu, W.; Tao, J.; Ma, N.; Zhao, C.; Shao, M. A Review on Laboratory Studies and Field Measurements of Atmospheric Organic Aerosol Hygroscopicity and Its Parameterization Based on Oxidation Levels. *Curr. Pollut. Reports* **2020**, *6* (4), 410–424. https://doi.org/10.1007/s40726-020-00164-2.

(91) Ng, N. L.; Brown, S. S.; Archibald, A. T.; Atlas, E.; Cohen, R. C.; Crowley, J. N.; Day, D. A.; Donahue, N. M.; Fry, J. L.; Fuchs, H.; Griffin, R. J.; Guzman, M. I.; Herrmann, H.; Hodzic, A.; Iinuma, Y.; Jimenez, J. L.; Kiendler-Scharr, A.; Lee, B. H.; Luecken, D. J.; Mao, J. Q.; McLaren, R.; Mutzel, A.; Osthoff, H. D.; Ouyang, B.; Picquet-Varrault, B.; Platt, U.; Pye, H. O. T.; Rudich, Y.; Schwantes, R. H.; Shiraiwa, M.; Stutz, J.; Thornton, J. A.; Tilgner, A.; Williams, B. J.; Zaveri, R. A. Nitrate Radicals and Biogenic Volatile Organic Compounds: Oxidation, Mechanisms, and Organic Aerosol. *Atmos. Chem. Phys.* **2017**, *17* (3), 2103–2162. https://doi.org/10.5194/acp-17-2103-2017.

(92) Mcdonald, J. D.; Zielinska, B.; Fujita, E. M.; Sagebiel, J. C.; Chow, J. C.; Watson, J. G. Fine Particle and Gaseous Emission Rates from Residential Wood Combustion. *Environ. Sci. Technol.* **2000**, *34* (11), 2080–2091. https://doi.org/10.1021/es9909632.

(93) Hays, M. D.; Geron, C. D.; Linna, K. J.; Smith, N. D.; Schauer, J. J. Speciation of Gas-Phase and Fine Particle Emissions from Burning of Foliar Fuels. *Environ. Sci. Technol.* **2002**, *36* (11), 2281–2295. https://doi.org/10.1021/es0111683.

(94) Mazzoleni, L. R.; Zielinska, B.; Moosmüller, H. Emissions of Levoglucosan, Methoxy

Phenols, and Organic Acids from Prescribed Burns, Laboratory Combustion of Wildland Fuels, and Residential Wood Combustion. *Environ. Sci. Technol.* **2007**, *41* (7), 2115–2122. https://doi.org/10.1021/es061702c.

(95) Simpson, C. D.; Paulsen, M.; Dills, R. L.; Liu, L. J. S.; Kalman, D. A. Determination of Methoxyphenols in Ambient Atmospheric Particulate Matter: Tracers for Wood Combustion. *Environ. Sci. Technol.* **2005**, *39* (2), 631–637. https://doi.org/10.1021/es0486871.

(96) Huang, Y.; Mahrt, F.; Xu, S.; Shiraiwa, M.; Zuend, A.; Bertram, A. K. Coexistence of Three Liquid Phases in Individual Atmospheric Aerosol Particles. *Proc. Natl. Acad. Sci. U. S. A.* **2021**, *118* (16). https://doi.org/10.1073/pnas.2102512118.

(97) Boyd, C. M.; Sanchez, J.; Xu, L.; Eugene, A. J.; Nah, T.; Tuet, W. Y.; Guzman, M. I.; Ng, N. L. Secondary Organic Aerosol Formation from the β-Pinene+NO3 System: Effect of Humidity and Peroxy Radical Fate. *Atmos. Chem. Phys.* **2015**, *15* (13), 7497–7522. https://doi.org/10.5194/acp-15-7497-2015.

(98) Lambe, A. T.; Wood, E. C.; Krechmer, J. E.; Majluf, F.; Williams, L. R.; Croteau, P. L.; Cirtog, M.; Féron, A.; Petit, J. E.; Albinet, A.; Jimenez, J. L.; Peng, Z. Nitrate Radical Generation via Continuous Generation of Dinitrogen Pentoxide in a Laminar Flow Reactor Coupled to an Oxidation Flow Reactor. *Atmos. Meas. Tech.* **2020**, *13* (5), 2397–2411. https://doi.org/10.5194/amt-13-2397-2020.

(99) Decarlo, P. F.; Kimmel, J. R.; Trimborn, A.; Northway, M. J.; Jayne, J. T.; Aiken, A. C.; Gonin, M.; Fuhrer, K.; Horvath, T.; Docherty, K. S.; Worsnop, D. R.; Jimenez, J. L. Aerosol Mass Spectrometer. *Anal. Chem.* **2006**, *78* (24), 8281–8289. https://doi.org/8410.1029/2001JD001213.Analytical.

(100) Takeuchi, M.; Ng, N. L. Chemical Composition and Hydrolysis of Organic Nitrate Aerosol Formed from Hydroxyl and Nitrate Radical Oxidation of α-Pinene and β-Pinene. *Atmospheric Chemistry and Physics*. 2019, pp 12749–12766. https://doi.org/10.5194/acp-19-12749-2019.

(101) Liu, P.; Song, M.; Zhao, T.; Gunthe, S. S.; Ham, S.; He, Y.; Qin, Y. M.; Gong, Z.; Amorim, J. C.; Bertram, A. K.; Martin, S. T. Resolving the Mechanisms of Hygroscopic Growth and Cloud Condensation Nuclei Activity for Organic Particulate Matter. *Nat. Commun.* **2018**, *9* (1). https://doi.org/10.1038/s41467-018-06622-2.

(102) Murray, B. J.; Haddrell, A. E.; Peppe, S.; Davies, J. F.; Reid, J. P.; O'Sullivan, D.; Price, H. C.; Kumar, R.; Saunders, R. W.; Plane, J. M. C.; Umo, N. S.; Wilson, T. W. Glass Formation and Unusual Hygroscopic Growth of Iodic Acid Solution Droplets with Relevance for Iodine Mediated Particle Formation in the Marine Boundary Layer. *Atmos. Chem. Phys.* **2012**, *12* (18), 8575–8587. https://doi.org/10.5194/acp-12-8575-2012.

(103) Renbaum-Wolff, L.; Grayson, J. W.; Bateman, A. P.; Kuwata, M.; Sellier, M.; Murray, B. J.; Shilling, J. E.; Martin, S. T.; Bertram, A. K. Viscosity of A-Pinene Secondary Organic Material and Implications for Particle Growth and Reactivity. *Proc. Natl. Acad. Sci. U. S. A.* **2013**, *110* (20), 8014–8019. https://doi.org/10.1073/pnas.1219548110.

(104) Grayson, J. W.; Song, M.; Sellier, M.; Bertram, A. K. Validation of the Poke-Flow Technique Combined with Simulations of Fluid Flow for Determining Viscosities in Samples with Small Volumes and High Viscosities. *Atmos. Meas. Tech.* **2015**, *8* (6), 2463–2472. https://doi.org/10.5194/amt-8-2463-2015.

(105) Rastak, N.; Pajunoja, A.; Acosta Navarro, J. C.; Ma, J.; Song, M.; Partridge, D. G.; Kirkevåg, A.; Leong, Y.; Hu, W. W.; Taylor, N. F.; Lambe, A.; Cerully, K.; Bougiatioti, A.; Liu, P.; Krejci, R.; Petäjä, T.; Percival, C.; Davidovits, P.; Worsnop, D. R.; Ekman, A. M. L.; Nenes, A.; Martin, S.; Jimenez, J. L.; Collins, D. R.; Topping, D. O.; Bertram, A. K.; Zuend, A.; Virtanen, A.; Riipinen, I. Microphysical Explanation of the RH-Dependent Water Affinity of Biogenic Organic Aerosol and Its Importance for Climate. *Geophys. Res. Lett.* **2017**, *44* (10), 5167–5177. https://doi.org/10.1002/2017GL073056.

(106) Renbaum-Wolff, L.; Song, M.; Marcolli, C.; Zhang, Y.; Liu, P. F.; Grayson, J. W.; Geiger, F. M.; Martin, S. T.; Bertram, A. K. Observations and Implications of Liquid-Liquid Phase Separation at High Relative Humidities in Secondary Organic Material Produced by α-Pinene Ozonolysis without Inorganic Salts. *Atmos. Chem. Phys.* **2016**, *16* (12), 7969–7979. https://doi.org/10.5194/acp-16-7969-2016.

(107) Suda, S. R.; Petters, M. D.; Yeh, G. K.; Strollo, C.; Matsunaga, A.; Faulhaber, A.; Ziemann, P. J.; Prenni, A. J.; Carrico, C. M.; Sullivan, R. C.; Kreidenweis, S. M. Influence of Functional Groups on Organic Aerosol Cloud Condensation Nucleus Activity. *Environ. Sci. Technol.* **2014**, *48* (17), 10182–10190. https://doi.org/10.1021/es502147y.

(108) Smith, N. R.; Crescenzo, G. V; Bertram, A. K.; Nizkorodov, S. A.; Faiola, C. L. Insect Infestation Increases Viscosity of Biogenic Secondary Organic Aerosol. *ACS Earth Sp. Chem* **2023**, *7* (5), 1060–1071. https://doi.org/10.1021/acsearthspacechem.3c00007.

(109) Baboomian, V. J.; Crescenzo, G. V.; Huang, Y.; Mahrt, F.; Shiraiwa, M.; Bertram, A. K.; Nizkorodov, S. A. Sunlight Can Convert Atmospheric Aerosols into a Glassy Solid State and Modify Their Environmental Impacts. *Proc. Natl. Acad. Sci. U. S. A.* **2022**, *119* (43), 1–10. https://doi.org/10.1073/pnas.2208121119.

(110) Smith, N. R.; Crescenzo, G. V; Huang, Y.; Hettiyadura, A. P. S.; Siemens, K.; Li, Y.; Faiola, C. L.; Laskin, A.; Shiraiwa, M.; Bertram, A. K.; Nizkorodov, S. A. Viscosity and Liquid–Liquid Phase Separation in Healthy and Stressed Plant SOA. *Environ. Sci. Atmos.* **2021**, *1* (3), 140–153. https://doi.org/10.1039/d0ea00020e.

(111) Song, M.; Maclean, A. M.; Huang, Y.; Smith, N. R.; Blair, S. L.; Laskin, J.; Laskin, A.; DeRieux, W.-S. W.; Li, Y.; Shiraiwa, M.; Nizkorodov, S. A.; Bertram, A. K. Liquid–Liquid Phase Separation and Viscosity within Secondary Organic Aerosol Generated from Diesel Fuel Vapors. *Atmos. Chem. Phys.* **2019**, *19* (19), 12515–12529. https://doi.org/10.5194/acp-19-12515-2019.

(112) Song, M.; Liu, P. F.; Hanna, S. J.; Zaveri, R. A.; Potter, K.; You, Y.; Martin, S. T.; Bertram, A. K. Relative Humidity-Dependent Viscosity of Secondary Organic Material from Toluene Photo-Oxidation and Possible Implications for Organic Particulate Matter over Megacities. *Atmos. Chem. Phys.* **2016**, *16* (14), 8817–8830. https://doi.org/10.5194/acp-16-8817-2016.

(113) Gregson, F. K. A.; Gerrebos, N. G. A.; Schervish, M.; Nikkho, S.; Schnitzler, E. G.; Schwartz, C.; Carlsten, C.; Abbatt, J. P. D.; Kamal, S.; Shiraiwa, M.; Bertram, A. K. Phase Behavior and Viscosity in Biomass Burning Organic Aerosol and Climatic Impacts. **2023**. https://doi.org/10.1021/acs.est.3c03231.

(114) Maclean, A. M.; Smith, N. R.; Li, Y.; Huang, Y.; Hettiyadura, A. P. S.; Crescenzo, G. V.; Shiraiwa, M.; Laskin, A.; Nizkorodov, S. A.; Bertram, A. K. Humidity-Dependent Viscosity of Secondary Organic Aerosol from Ozonolysis of β-Caryophyllene: Measurements, Predictions, and Implications. *ACS Earth Sp. Chem.* **2021**, *5* (2), 305–318. https://doi.org/10.1021/acsearthspacechem.0c00296.

(115) Smith, N. R.; Crescenzo, G. V.; Huang, Y.; Hettiyadura, A. P. S.; Siemens, K.; Li, Y.; Faiola, C. L.; Laskin, A.; Shiraiwa, M.; Bertram, A. K.; Nizkorodov, S. A. Viscosity and Liquid-Liquid Phase Separation in Healthy and Stressed Plant SOA. *Environ. Sci. Atmos.* **2021**, *1* (3), 140–153. https://doi.org/10.1039/d0ea00020e.

(116) Grayson, J. W.; Evoy, E.; Song, M.; Chu, Y.; Maclean, A.; Nguyen, A.; Upshur, M. A.; Ebrahimi, M.; Chan, C. K.; Geiger, F. M.; Thomson, R. J.; Bertram, A. K. The Effect of Hydroxyl Functional Groups and Molar Mass on the Viscosity of Non-Crystalline Organic and Organic-Water Particles. *Atmos. Chem. Phys.* **2017**, *17* (13), 8509–8524. https://doi.org/10.5194/acp-17-8509-2017.

(117) Meng, L.; Coeur, C.; Fayad, L.; Houzel, N.; Genevray, P.; Bouzidi, H.; Tomas, A.; Chen, W. Secondary Organic Aerosol Formation from the Gas-Phase Reaction of Guaiacol (2-Methoxyphenol) with NO3 Radicals. *Atmos. Environ.* **2020**, *240* (June). https://doi.org/10.1016/j.atmosenv.2020.117740.

(118) C. A. Angell. Relaxation in Liquids, Polymers and Plastic Crystals - Strong/Fragile Patterns and Problems. *J. Non. Cryst. Solids* **1991**, *131*, 13–31.

(119) Maclean, A. M.; Li, Y.; Crescenzo, G. V.; Smith, N. R.; Karydis, V. A.; Tsimpidi, A. P.; Butenhoff, C. L.; Faiola, C. L.; Lelieveld, J.; Nizkorodov, S. A.; Shiraiwa, M.; Bertram, A. K. Global Distribution of the Phase State and Mixing Times within Secondary Organic Aerosol Particles in the Troposphere Based on Room-Temperature Viscosity Measurements. *ACS Earth Sp. Chem.* **2021**, *5* (12), 3458–3473. https://doi.org/10.1021/acsearthspacechem.1c00296.

(120) Jöckei, P.; Tost, H.; Pozzer, A.; Brühl, C.; Buchholz, J.; Ganzeveld, L.; Hoor, P.; Kerkweg, A.; Lawrence, M. G.; Sander, R.; Steil, B.; Stiller, G.; Tanarhte, M.; Taraborrelli, D.; Van Aardenne, J.; Lelieveld, J. The Atmospheric Chemistry General Circulation Model ECHAM5/MESSy1: Consistent Simulation of Ozone from the Surface to the Mesosphere. *Atmos. Chem. Phys.* **2006**, *6* (12), 5067–5104. https://doi.org/10.5194/acp-6-5067-2006.

(121) Petters, S. S.; Kreidenweis, S. M.; Grieshop, A. P.; Ziemann, P. J.; Petters, M. D. Temperature- and Humidity-Dependent Phase States of Secondary Organic Aerosols. *Geophys. Res. Lett.* **2019**, *46* (2), 1005–1013. https://doi.org/10.1029/2018GL080563.

(122) Atkinson, R.; Baulch, D. L.; Cox, R. A.; Crowley, J. N.; Hampson, R. F.; Hynes, R. G.; Jenkin, M. E.; Rossi, M. J.; Troe, J. Evaluated Kinetic and Photochemical Data for

Atmospheric Chemistry: Volume I - Gas Phase Reactions of O_x, HO_x, NO_x and SO_x Species. *Atmos. Chem. Phys.* **2004**, *4* (6), 1461–1738. https://doi.org/10.5194/acp-4-1461-2004.

(123) Shrivastava, M.; Lou, S.; Zelenyuk, A.; Easter, R. C.; Corley, R. A.; Thrall, B. D.; Rasch, P. J.; Fast, J. D.; Simonich, S. L. M.; Shen, H.; Tao, S. Global Long-Range Transport and Lung Cancer Risk from Polycyclic Aromatic Hydrocarbons Shielded by Coatings of Organic Aerosol. *Proc. Natl. Acad. Sci. U. S. A.* **2017**, *114* (6), 1246–1251. https://doi.org/10.1073/pnas.1618475114.

(124) Evoy, E.; Maclean, A. M.; Rovelli, G.; Li, Y.; Tsimpidi, A. P.; Karydis, V. A.; Kamal, S.; Lelieveld, J.; Shiraiwa, M.; Reid, J. P.; Bertram, A. K. Predictions of Diffusion Rates of Large Organic Molecules in Secondary Organic Aerosols Using the Stokes-Einstein and Fractional Stokes-Einstein Relations. *Atmos. Chem. Phys.* **2019**, *19* (15), 10073–10085. https://doi.org/10.5194/acp-19-10073-2019.

(125) Lilek, J.; Zuend, A. A Predictive Viscosity Model for Aqueous Electrolytes and Mixed Organic-Inorganic Aerosol Phases. *Atmos. Chem. Phys.* **2022**, *22* (5), 3203–3233. https://doi.org/10.5194/acp-22-3203-2022.

(126) Gorkowski, K.; Donahue, N. M.; Sullivan, R. C. Aerosol Optical Tweezers Constrain the Morphology Evolution of Liquid-Liquid Phase-Separated Atmospheric Particles. *Chem* **2020**, *6* (1), 204–220. https://doi.org/10.1016/j.chempr.2019.10.018.

(127) Gorkowski, K.; Preston, T. C.; Zuend, A. Relative-Humidity-Dependent Organic Aerosol Thermodynamics via an Efficient Reduced-Complexity Model. *Atmos. Chem. Phys.* **2019**, *19* (21), 13383–13407. https://doi.org/10.5194/acp-19-13383-2019.

(128) Ye, J.; Gordon, C. A.; Chan, A. W. H. Enhancement in Secondary Organic Aerosol Formation in the Presence of Preexisting Organic Particle. *Environ. Sci. Technol.* **2016**, *50* (7), 3572–3579. https://doi.org/10.1021/acs.est.5b05512.

(129) Mahrt, F.; Peng, L.; Zaks, J.; Huang, Y.; Ohno, P. E.; Smith, N. R.; Gregson, F. K. A.; Qin, Y.; Faiola, C. L.; Martin, S. T.; Nizkorodov, S. A.; Ammann, M.; Bertram, A. K. Not All Types of Secondary Organic Aerosol Mix: Two Phases Observed When Mixing Different Secondary Organic Aerosol Types. *Atmos. Chem. Phys.* **2022**, *22* (20), 13783–13796. https://doi.org/10.5194/acp-22-13783-2022.

(130) Petters, M.; Kasparoglu, S. Predicting the Influence of Particle Size on the Glass Transition Temperature and Viscosity of Secondary Organic Material. *Sci. Rep.* **2020**, *10* (1). https://doi.org/10.1038/s41598-020-71490-0.

(131) Crittenden, J. C.; Trussell, R. R.; Hand, D. W.; Howe, K. J.; Tchobanoglous, G. *MWH's Water Treatment: Principles and Design*; John Wiley & Sons, 2012.